Environmental Science: Atmospheres

ROYAL SOCIETY OF CHEMISTRY

PAPER

View Article Online
View Journal | View Issue

Check for updates

Cite this: *Environ. Sci.: Atmos.*, 2023, **3**, 1460

Bimolecular sinks of Criegee intermediates derived from hydrofluoroolefins – a computational analysis†

Nathan A. I. Watson *[ab] and Joseph M. Beames [ac]

A novel range of stabilised Criegee intermediate (sCI) species with halogenated substituent groups have been identified as products to the reaction between with gaseous ozone and hydrofluoroolefins (HFOs), a series of recently-developed and increasingly prevalent haloalkene refrigerants. The bimolecular chemistry of this group of hydrofluoroolefin-derived sCIs (HFO-sCIs) has yet to be explored in any significant detail so this work evaluates the reaction chemistry of common tropospheric gaseous species with the following group of HFO-sCIs: *syn*- & *anti*-CF_3CHOO & *syn*- & *anti*-CF_3CFOO. Using high-level theoretical calculations (DF-HF/DF-LCCSD(T)-F12a//B3LYP/aug-cc-pVTZ), this study demonstrates that HFO-sCIs will deplete many pollutants (*e.g.* HCHO, SO_2 & H_2S) but also act as a source of other atmospheric contaminants (*e.g.* SO_3 & TFA). The bimolecular reactivity of the HFO-sCIs were compared against CH_2OO, the most frequently studied sCI, for which the general reactivity trend has been identified: k_{THEO} (*syn*-CF_3CHOO) < k_{THEO} (*anti*-CF_3CHOO) ≈ k_{THEO} (CH_2OO) ≪ k_{THEO} (*anti*-CF_3CFOO) < k_{THEO} (*syn*-CF_3CFOO). In general *syn* & *anti*-CF_3 substituents reduce overall sCI reactivity compared to similar non-halogenated sCI species, whereas both *syn* & *anti*-F substituents significantly increase HFO-sCI reactivity. While HFO-sCI reactivity is largely dictated by the identity and location of the sCI substituent groups, there are co-reactants that alter these observed trends in reactivity, for example HCl reacts more rapidly with CH_2OO than it does with *syn*- & *anti*-CF_3CFOO.

Received 29th June 2023
Accepted 15th August 2023

DOI: 10.1039/d3ea00102d

rsc.li/esatmospheres

Open Access Article. Published on 17 srpna 2023. Downloaded on 07.01.2026 15:12:46.
This article is licensed under a Creative Commons Attribution 3.0 Unported Licence.

Environmental significance

Emissions of new short-lived hydrofluoroolefin coolants have become increasingly widespread in the last decade and the breakdown of these hydrofluoroolefins will generate many secondary products, including a range of hydrofluoroolefin-derived stabilised Criegee intermediates (HFO-sCIs). Criegee intermediates are important OH radical sources and strong tropospheric sinks for many pollutants, but HFO-sCI reactivity has not yet been fully characterised. This computation chemistry study provides a greater understanding of the implications of the increased tropospheric HFO-sCI abundance. The enhanced bimolecular reactivity found for HFO-sCIs in this study indicates that several of the HFO-sCIs have heightened capacities to: react with toxins (*e.g.* methanol & trifluoroacetic acid); produce hydroperoxides implicated with forestry damage; and convert SO_2 to SO_3, a process implicated with generating H_2SO_4 and aerosols.

1 Introduction

The recent commercialisation of highly volatile hydrochlorofluoroolefins and hydrofluoroolefins (referred to collectively herein as HFOs) for use as coolants in refrigerator units have been developed to reduce greenhouse gas emissions and reduce stratospheric ozone loss.[1–6] Furthermore, as well as being used as blowing foam and as propellants, HFOs are very important working fluids for waste heat recovery applications in heat pumps, as they are stable, have favourable toxicity profiles and are compatible with many plastics and elastomers used in such set-ups.[7,8] When haloalkenes breakdown it is the Cl & Br radicals that are primarily implicated in ozone destruction in the upper atmosphere and therefore only HFOs containing Cl & Br atoms (*e.g.* HCFO-1233zd(*E*)) appear to marginally affect stratospheric ozone levels.[9–12] But their compact lifetime means HFOs

[a]*School of Chemistry, Main Building, Cardiff University, Cardiff, CF10 3AT, UK. E-mail: nathan.watson@manchester.ac.uk*

[b]*Department of Earth and Environmental Sciences, Simon Building, University of Manchester, Manchester, M13 9PS, UK*

[c]*School of Chemistry, Main Building, Edgbaston, Birmingham, B15 2TT, UK*

† Electronic supplementary information (ESI) available: A full breakdown of the master equation rate constants (k_{ME}) and canonical rate constants (k_{CAN}) through temperature range of 200 K < T < 500 K at p = 760 Torr for **sCIs 1–5** reactions with the following co-reactants: HCHO, SO_2, HNO_3, TFA, HF, HCl, H_2S, H_2O, $(H_2O)_2$, MeOH; calculated product yields for **sCIs 1–5** reactions with HCHO, SO_2; calculated values for **sCI 1** + co-reactant rate constants at selected temperatures and pressures for direct comparison with experiment; calculated values for the effective rate constants for sCI + co-reactant reactions under various conditions; relative energies [kJ mol^{-1}] of stationary point for sCI + co-reactant reactions; computed dipole–dipole and gas collision limits; discussion on the partially barrierless **sCI 4** + MeOH reaction; Cartesian coordinates and vibrational frequencies of all stationary points, and IRCs of all transition states in this study; an example MEMSER input file for the **sCI 1** + HNO_3 (PDF). See DOI: https://doi.org/10.1039/d3ea00102d

© 2023 The Author(s). Published by the Royal Society of Chemistry

Open Access Article. Published on 17 srpna 2023. Downloaded on 07.01.2026 15:12:46.
This article is licensed under a Creative Commons Attribution 3.0 Unported Licence.

are often depleted in the troposphere and contribute to only minimal ozone depletion.[9–12] Additionally, they are relatively non-toxic, have minimal impact on global warming due to their short lifespans, and have high ignition energies compared to the first generation of refrigerants used in the 19th century (*e.g.* NH_3, SO_2 & CH_3CHO).[1–3,13–17] Moreover, whereas CO_2 dominates the lower IR wave numbers (600–750 cm^{-1}), HFCs/HCFCs are also strongly IR active in the higher wavenumbers (1000–1400 cm^{-1}), increasing their heat trapping ability.[9,18] In contrast, the longevity of the second-generation chlorofluorocarbon (CFC) refrigerants leads to depletion of stratospheric O_3, which results in more cases of skin cancer from the greater ground-level penetration of the carcinogenic high-frequency UV light.[19–21]

The growing interest in alternative refrigerants stems from the fact that, while the hydrofluorocarbon (HFC) and hydrochlorofluorocarbon (HCFC) replacements that have been phased in since the 1970s do not replicate this ozone depletion, the lengthy lifetimes and high levels of IR activity of HFCs & HCFCs give them very high global warming potentials (GWP_{100}).[2,9,19,22–26] In areas as widespread as China, the USA and the EU, the phasing in of HFOs has been increasingly integrated into regional regulations, to try and eliminate HCFC & HFC emissions, and this has led to HFOs seeing increasing use in refrigerators, insulation and vehicle cooling units.[1,27,28] For example, a UK government 2022 report on the "F gas regulation in Great Britain" documents that HFO-1234yf has dominated total refrigerant usage in new small vehicles since 2017 and HFO–HFC blends use could eliminate high GWP HFCs from transport refrigeration by 2050.[29] Modest concerns about both the tropospheric implications of HFO breakdown (*e.g.* TFA formation) and about the carbon-intensity of HFO production has meant that both the UK and the EU are currently assessing the role of HFOs in future climate regulations.[30] Many refrigerant experts and industrial leaders continue to strongly support HFO use and are consulting on such regulations with governments currently, especially as the alternatives to HFOs also have trade-offs in the areas of toxicity, flammability and/or high-pressure requirements.[31,32] Examples of CFCs, HCFCs, HFCs and HFOs with their GWP_{100} and ODP values and lifespan are displayed in Table 1.

One of the reasons for the short-lived nature of HFOs listed in Table 1, HFO-1234yf, HCFO-1233zd(E) and HFO-1234ze(E), all of which are now widely used as refrigerants or insulation foam, is that the unsaturated ⟩C=C⟨ bond makes HFOs more susceptible to these chemical loss mechanisms.[1,3–5,27,35–39] The gas-phase reaction of HFOs with radicals, such as OH & Cl, and other reactive species, like O_3, are important atmospheric loss mechanisms for many such tropospheric alkenes, for example isoprene reaction with O_3 is responsible for ~10% of the loss of this non-halogenated alkene globally.[4–6,34,40–44] The importance of this HFO 'ozonolysis' loss process is increasing year-on-year because the rise of HFO emissions particularly in O_3-rich urban areas is likely to result in sizable increases tropospheric populations of the Criegee intermediate (CI) and aldehyde/ketone products of this process (see Fig. 1).[4,5,45–48] A recent rise in tropospheric trifluoroacetic acid (TFA) abundance in Beijing has already been partially attributed to the reaction of OH radicals with HFOs and, as a similar increase in other HFO-derived products is likely in similar circumstances, determining the tropospheric impact these of new HFO-derived stabilised Criegee intermediates (HFO-sCIs) is very necessary.[3,28,36,49–51]

The efficiency of ozonolysis as a tropospheric depletion mechanism for HFOs is disputed because while the presence of halogenated groups in the HFO reduces the overall effectiveness of most major alkene depletion pathways, such as *via* reaction with OH or Cl, this varies considerably depending on the HFO.[45–47,52,53] The maximum ozonolysis yield for most HFOs reviewed are around 1%, but a few studies indicate that up to 10% of the removal of some haloalkenes occur *via* reaction with O_3, a significant enough pathway that HFO ozonolysis is being

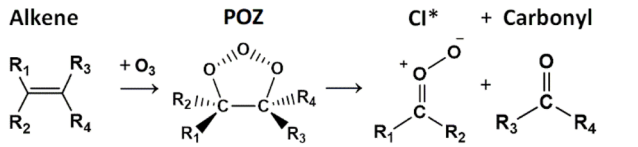

Fig. 1 The general schematic for the ozonolysis of a standard alkene *via* a short-lived primary ozonide (POZ) intermediate products, which produces in a pair of final products: a Criegee intermediate (CI) and a carbonyl product (either aldehyde or ketone). A significant portion of the CI population is formed with a high degree of energy indicated by asterisk.

Table 1 A tabulation of important atmospheric attributes of examples from three different generations of refrigerants: chlorofluorocarbon (CFCs), hydrofluorocarbons (HFCs) and hydrofluoroolefins (HFOs). Attributes featured include: global warming potential over 100 years (GWP_{100}), ozone depletion potential (ODP), atmospheric lifetime, and any hydrofluoroolefin-derived stabilized Criegee intermediates (HFO-sCIs) produced from the ozonolysis of this species

Name	Structure	GWP_{100}	ODP	Lifetime (year)	HFO-sCIs	Ref.
HFO-1234yf	$CF_3CF{=}CH_2$	4	0	10.5 days	CH_2OO *Syn*-/*anti*-CF_3CFOO	2, 4 and 9
HCFO-1233zd(E)	E-$CF_3CH{=}CHCl$	14	0.0005	26 days	*Syn*-/*anti*-ClCHOO *Syn*-/*anti*-CF_3CHOO	2, 5 and 33
HFO-1234ze(E)	E-$CF_3CH{=}CHF$	<1	0	16.4 days	*Syn*-/*anti*-FCHOO *Syn*-/*anti*-CF_3CHOO	2, 9 and 34
CFC-11	$CFCl_3$	4660	1	45	—	2 and 9
CFC-12	CCl_2F_2	10 200	0.82	100	—	2
HFC-134a	CF_3CH_2F	3710	0.0013	13.4	—	2 and 26
HFC-245fa	$CF_3CH_2CHF_2$	858	0	7.7	—	2 and 9

© 2023 The Author(s). Published by the Royal Society of Chemistry

Open Access Article. Published on 17 srpna 2023. Downloaded on 07.01.2026 15:12:46.
This article is licensed under a Creative Commons Attribution 3.0 Unported Licence.

investigated thoroughly at present.[47,52] Furthermore, while direct CI branching fraction measurements for HFO ozonolysis are not found in the literature, indirect measurements of their aldehyde/ketone co-products show strong yields for CF_3CHOO species and other similar CIs (>40%).[52,54] This indicates that ozonolysis of haloalkenes in general are a major pathway for producing HFO-sCIs, even if these halogenated sCIs are low in abundance and ozonolysis is not the dominant pathway for removal of HFOs. This is a highly important topic and of relevance to the study of Criegee intermediates. Relative HFO ozonolysis percentages have been avoided here due to this need for a much more thorough re-investigation.

CIs are produced from the ozonolysis of a large variety of both halo-alkenes and non-halogenated alkenes and the atmospheric role of these CIs have been the subject of increased scientific study in the literature in recent years.[5,6,34,48] This is due to the fact that a large portion of the CIs produced by alkene ozonolysis (35–50%) are formed with such excess of internal energy that they undergo a rapid unimolecular fragmentation process, which is an important non-photolytic source of the atmospheric 'detergent' HO˙ species. The remaining fraction are stabilised by collision, generating stabilised Criegee intermediates (sCIs), that can participate in bimolecular reactions with other atmospheric species. These sCIs deplete pollutants to such an extent that the simplest sCI, formaldehyde oxide (CH_2OO), can compete with the atmospheric "detergent" HO˙ species as a sink for polar pollutants, such as HNO_3 and SO_2, especially in CH_2OO-rich boreal forest environments ([CH_2OO] $\sim 1–5 \times 10^4$ molec. per cm^3).[42,55] To examine the capacity of sCIs to deplete pollutants is the purpose of this study, as well as much of the increased scientific examination of sCIs overall.

The theoretical literature (see Table 1) shows that the ozonolysis of prominent HFOs produces several particular HFO-derived stabilised Criegee intermediates (HFO-sCIs): CH_2OO, *syn*- & *anti*-FCHOO, *syn*- & *anti*-ClCHOO, *syn*- & *anti*-CF_3CHOO and *syn*- & *anti*-CF_3CFOO.[4,5,45,46,53,56] Only the bimolecular chemistry of CH_2OO species has been explored in the experimental literature, although *syn*- & *anti*-CF_3CHOO and *syn*- & *anti*-ClCHOO have been experimentally identified.[57–66] In a small number of studies, the bimolecular chemistry of HFO-sCIs has been interrogated using computational chemistry techniques: CH_2OO somewhat exhaustively;[67–71] *syn*- & *anti*-FCHOO and *syn*- & *anti*-ClCHOO in reactions with CO_2, H_2, MeOH and CH_4;[72–76] and *syn*- & *anti*-CF_3CHOO in reactions with CO_2, $CF_3CH{=}CH_2$ and H_2.[72,73,77] The literature has very little analysis of *syn*- or *anti*-CF_3CFOO. As much of the bimolecular chemistry of *syn*- & *anti*-FCHOO and *syn*- & *anti*-ClCHOO has already been previously studied in the computational literature, the HFO-sCIs explored herein are instead CH_2OO, *syn*-CF_3CHOO, *anti*-CF_3CHOO, *syn*-CF_3CFOO and *anti*-CF_3CFOO, which are labelled as **sCIs 1–5** and are displayed in Fig. 2.[72–75]

Also displayed in Fig. 2 is the targeted range of co-reactants selected for this computational study, including both H_2O & $(H_2O)_2$ because the global abundance of water vapour (~0–40 000 ppm) means that these molecules are responsible for reacting with up to 95% of the total global flux of some atmospheric sCIs.[67,68,78–83] As shown previously with the high abundance of TFA in Beijing, HFO breakdown produces a variety of

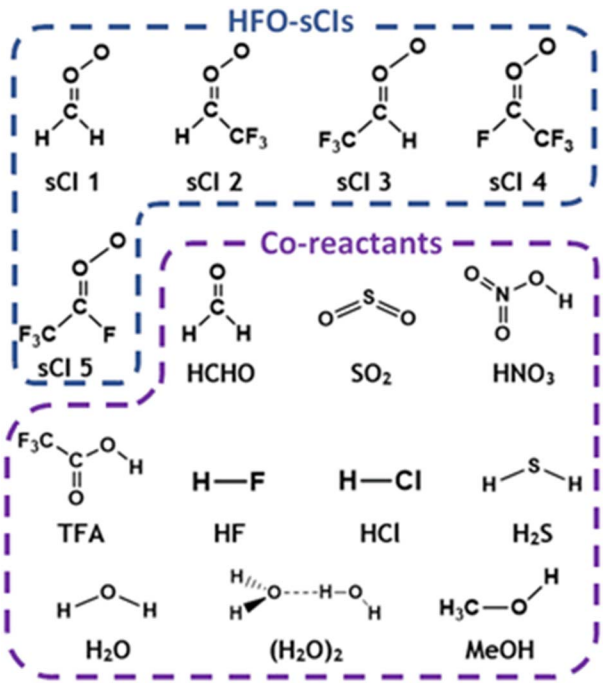

Fig. 2 Geometric structures of hydrofluoroolefin-derived stabilised Criegee intermediates, HFO-sCIs, labelled as **sCIs 1–5**, and co-reactants examined in this in this study. In each case, rate constants for each HFO-sCI + co-reactant reaction are evaluated.

secondary products, including HCHO, and so both TFA & HCHO are studied here as they like to have significant overlapping local concentrations with HFO-sCIs.[3,4,28,36,49–51]

Some co-reactants (HNO_3, HCl & H_2S) are selected for study here because there are some environments in which CH_2OO competes with OH radicals to facilitate the depletion of these co-reactants, as noted by Khan *et al.*[42] Furthermore, some co-reactants studied here, such as SO_2, are of interest because their reactions with sCIs are a competitive source for tropospherically relevant species such as SO_3, which is considered vital in aerosol nucleation pathways.[84,85] Another example is that sCI + MeOH & H_2O reactions produce a large proportion of the global flux of the α-alkoxyalkylhydroperoxides (AAAH) and α-hydroxy-hydroperoxides (HHP). These are oxidising species that cause both forest damage and SOA formation.[67,68,72,78–80,83,86]

One last area of consideration in co-reactant targeting is that Kumar *et al.* propose that sCI reactivity with H_2X (X = O, S, Se, and Te) increases with the size of the X atom, referred to as heteroatom tuning of the co-reactants.[87] In this study, the co-reactants with low mass heteroatoms, H_2O & HF, are compared with species which have the same structures but larger heteroatoms of the same periodic group, H_2S & HCl, to see if all the HFO-sCIs in this chapter replicate the co-reactant heteroatom tuning patterns observed in the Kumar *et al.* study.[87] The last reactions featured are examined because the HCHO + **sCIs 2** & **3** and **sCI 1** + CF_3CHO reactions are part of the same multistep potential energy surface (PES) and so the theoretical rate constants (k_{THEO}) and product branching ratios (Γ_{THEO}) of **sCI 1** + CF_3CHO can be determined with little additional computational cost. This is also the case for

© 2023 The Author(s). Published by the Royal Society of Chemistry

Open Access Article. Published on 17 srpna 2023. Downloaded on 07.01.2026 15:12:46.
This article is licensed under a Creative Commons Attribution 3.0 Unported Licence.

HCHO + **sCIs 4** & **5** and **sCI 1** + CF_3CFO reactions which are all part of the same multistep potential energy surface.

By using computational chemistry methods to review reactions with this variety of common tropospheric gas species, this study aims to evaluate to what degree the bimolecular chemistry of HFO-sCI (*syn*- & *anti*-CF_3CHOO and *syn*- & *anti*-CF_3CFOO) differs from that of CH_2OO, as well as the other non-halogenated sCIs.

2 Methodologies

This work employs a density functional theory (DFT) approach, using the hybrid B3LYP functional, and the Dunning correlation-consistent aug-cc-pVTZ basis set (B3LYP/aug-cc-pVTZ), is used to optimise the geometric structures of all minimum and transition state (TS) geometries, referred to collectively as stationary points.[88–99] Each minimum or TS structure is verified through evaluation of the number of imaginary frequencies from subsequent harmonic frequency calculations, performed at the same level of theory as the optimisation. TSs identified in this manner are mapped to the geometric minima that they bisect using intrinsic reaction coordinate (IRC) calculations. For very shallow TSs and barrierless reactions, IRC calculations become computationally challenging, therefore in these cases relaxed potential energy scans are performed using incremental separation of a molecular bond (which forms a key component of the reaction coordinate) until the local minima is reached. The relax surface scans for non-barrierless channels each have a local energy maximum, which denote the location of the TS structure on the potential energy surface, whereas the energy diagram for barrierless channels only display asymptotic Morse-like behaviour. Optimisations, harmonic frequencies, IRCs and potential energy scans are all performed using the Gaussian09 computational chemistry programme.[100] All optimisations in this study were performed on singlet surfaces.

Rate constants and PESs are constructed by using DFT optimised structures with energies refined using a higher level, *ab initio* approach. Single point molecular energy calculations, for all stationary points, are calculated using a localised, density fitted coupled cluster method with the same Dunning basis set (DF-HF/DF-LCCSD(T)-F12a/aug-cc-pVTZ).[91,94–96,101–111] These molecular energies are calculated in the MOLPRO computational chemistry package.[112] All zero-point energies or Gibbs free energies in this study are calculated using the zero-point and free energy corrections acquired from the DFT harmonic frequency calculations. All relative energies (ΔE) referenced herein in the main body of this manuscript and in all PESs are zero-point corrected. This overall computational approach, when applied to the variety of sizes of sCIs and co-reactants in this study, provides both accurate energies and manageable computational cost. This computational approach is used in other studies in the literature too and it effectively describes the chemistry of sCI reactions with TFA & alcohols.[61,74] For further verification of the veracity of this computational approach, the theoretical rate constants (k_{THEO}) for the bimolecular **sCI 1** reactions obtained in this study are benchmarked against experimental rate constants (k_{EXP}) from the literature.

The open source Master Equation Solver for Multi-Energy Well Reactions (MESMER) software is used to calculate the microcanonical kinetic reaction rates by deriving the individual energy-grained master equation (EGME) rate coefficients, which are then subsequently used to generate the overall master equation rate constant (k_{THEO}) and product branching ratios (Γ_{THEO}) of the system over a range of temperatures.[113] Computational chemistry rate constants from other studies are also referred to as k_{THEO} constants, even if generated using differing methods. Master equation rate constants are referred to as k_{ME} values only in the ESI† to distinguish them from other theoretical rate constants. This software has been used extensively to solve analogous chemical problems, and has been utilised previously to evaluate Criegee intermediate reaction kinetics.[76,84,114–119]

These MESMER calculations include a rigid rotor harmonic oscillator approximation, with structures and vibrational frequencies again taken from the DFT calculations, as shown by the example MESMER input in ESI Section S9.†[113] An inverse Laplace transform (ILT) capture rate coefficient of 1×10^{-10} cm^3 s^{-1} and an excess reactant concentration of 1×10^{16} molecule cm^{-3} are assumed.[76,113] The collisional energy transfer factor, $\langle \Delta E_{down} \rangle$, was assigned as 300 cm^{-1} for all minima. This has been shown to be a good approximation for systems involving nitrogen as a gas bath.[76,113,120] A 10 cm^{-1} grain size was routinely used for the EGME calculations, however, for the larger systems, grain sizes are adjusted to reduce computational expense (ESI Sections 1.1–1.4†).

Low mass atom motion within the reaction mechanism is sometimes facilitated by quantum tunnelling, often accelerating the reaction. The effect of tunneling on the rate constant is determined herein using a non-*ab initio* tunneling correction called the asymmetrical Eckart constant (k_{ECKART}).[121] This k_{ECKART} is calculated and then integrated directly into the k_{THEO} and Γ_{THEO} values through the MESMER software package, unless the reaction barriers are too low to support this methodology (these exceptions are stated in the ESI Section S1.1†).[76,113,121] In calculating the k_{ECKART} function, the probability of transmission through the one-dimensional energy barrier, $p(E)$, needs to be calculated using eqn (1)–(7):

$$p(E) = 1 - \left[\frac{\cosh[2\pi(\alpha-\beta)] + \cosh[2\pi\delta]}{\cosh[2\pi(\alpha+\beta)] + \cosh[2\pi\delta]}\right] \quad (1)$$

$$\alpha = \frac{1}{2\sqrt{C}}\sqrt{E} \quad (2)$$

$$\beta = \frac{1}{2\sqrt{C}}\sqrt{E-A} \quad (3)$$

$$\delta = \frac{1}{2\sqrt{C}}\sqrt{B-C} \quad (4)$$

$$A = \Delta H_f^{\ddagger,0K} - \Delta H_r^{\ddagger} \quad (5)$$

$$B = \sqrt{\Delta H_f^{\ddagger,0K}} - \sqrt{\Delta H_r^{\ddagger,0K}} \quad (6)$$

Open Access Article. Published on 17 srpna 2023. Downloaded on 07.01.2026 15:12:46.
This article is licensed under a Creative Commons Attribution 3.0 Unported Licence.

$$C = (h.\mathrm{im}(\nu^{\ddagger}))^2 \left[\frac{B^3}{A^2 - B^2}\right]^2 \quad (7)$$

Calculating the probability of transmission involves estimating the barrier width between the reactants and products using: the forward and reverse zero-point corrected energy barriers, $\Delta H_f^{\ddagger,0K}$ and $\Delta H_r^{\ddagger,0K}$, and the imaginary frequency of the associated TS describing the reaction coordinate, $\nu^{\ddagger}$. The k_{ECKART} value is then determined using $p(E)$ in eqn (8):

$$k_{ECKART} = \frac{e^{\Delta H_f^{\ddagger,0K}}}{k_B T} \int_0^{\infty} p(E) e^{-\frac{E}{k_B T}} dE \quad (8)$$

The irreversible final product formation processes are accommodated by the MESMER software by means of using an infinite "sink" approximation. In a system where a particular reaction channel that produces multiple products *via* a post-reaction complex (*i.e.* reactant → TS → post-reaction complex → product 1 + product 2) herein the formation of the post-reaction complex is treated as irreversible by MESMER when determining the k_{ECKART} & Γ_{THEO} values and it is assumed that ~100% of this post-reaction complex separates into the final individual bimolecular products. This approximation reduces the computational intensity of MESMER calculations and introduces an error of less than 1%.[122,123] This use of the post-reaction complex can be seen in the MESMER example file in the ESI.†

In some multi-step reactions, a small number of the intermediate product → final products fragmentations involve progressing over an asymptotic Morse-like energy curve until the final separated products are formed, rather than fragmenting *via* a transition state. When Peltola *et al.* examined CH_2OO decomposing into HCO + OH and Blitz *et al.* studied CH_3NH breaking down into CH_3 + NH, both used a reverse inverse Laplace transformation (reverse ILT) method in MESMER to interpret these chemical pathways,[117,124] and both use the reverse ILT method with the experimental rate constant (k_{EXP}) of the equivalent forward reaction as the pre-exponential factor.[117,124] However, as the reaction channels in this study where the reverse ILT method is used have no literature k_{EXP} values instead the dipole–dipole capture limit rate constant, k_{d-d}, (discussed in the next paragraph) are used as the pre-exponential factors instead. Furthermore, this reverse ILT method requires using the term reverse = true in the activation energy component and assigning both final products as separate sink structures.

In a few previous studies, sCI reactions with other trace atmospheric species (*e.g.* **sCI 1** + HCOOH, CH_3COOH or CF_3COOH) have produced such large k_{THEO} & k_{EXP} values that each sCI + co-reactant collision leads to a reaction.[59–61,74,125] Under such conditions, it is proposed that k_{THEO} values can be more accurately modelled using a collision frequency model, such as the dipole–dipole capture limit, k_{d-d}. The k_{d-d} value is calculated using eqn (9) and (10):

$$k_{d-d} = C\sqrt{\pi/\mu}(\mu_{D1}\mu_{D2})^{(2/3)}(k_B T)^{-1/6} \quad (9)$$

$$\mu = \frac{m_1 m_2}{m_1 + m_2} \quad (10)$$

C is a constant dependent on the anisotropy of the capture potential; μ_{D1} and μ_{D2} are the dipole moments of reactants 1 & 2; and μ is the total reduced mass of the system calculated using the mass of reactants 1 & 2 (m_1 & m_2).[126] The C value adopted can be either isotropic (4.08), adiabatic anisotropic (2.68) and non-adiabatic anisotropic (1.953).[126] The isotropic k_{d-d} constant is used in this study, as it is much used in the literature for bimolecular sCI reactions.[61,125]

Frequently in this study, the rate determining step is barrierless or $k_{THEO} > k_{d-d}$ (usually where $k_{THEO} \geq \sim 10^{-10}$) and so the k_{d-d} is used as the overall rate constant, as it is a more true reflection of the tropospheric rate constant. As sCIs are polar in character, the isotropic k_{d-d} value is used over the more traditional collision limit (k_{COLL}) too, as k_{d-d} is better able to model the effect this polarity has on sCI — co-reactant collision frequency. However, the k_{COLL} values for each reaction, along with the adiabatic anisotropic and non-adiabatic anisotropic k_{d-d} values, are all listed in the ESI Section S3† for comparison. The rate constants generated in this work are analysed using the effective first-order rate constant, k_{EFF}, which accounts for the concentration of the co-reactant:[35]

$$k_{EFF} = k_{THEO}[\text{co-reactant}] \quad (11)$$

These k_{EFF} values in this work are calculated using previously reported co-reactant concentrations in example 'important' local environments. This data is displayed in Table 2 in the next section, alongside any known experimental rate constants for the same reactions. Further examples of other local co-reactant abundances in other environments and the effect they have on the k_{EFF} values are listed in ESI Section S4.†

3 Results & discussion

The bimolecular master equation rate constant (k_{THEO}), the dipole–dipole capture limit (k_{d-d}), and the effective rate constant (k_{EFF}), for the HFO-sCI reactions calculated in this study are found in Table 2. The co-reactant abundances featured in Table 2 are selected from locations where either the pollutant has a high enough concentration to be a potentially significant sCI sink and/or an area where humans may face a significant degree exposure of either the pollutant or the potential product of this reaction. These values are then used to generate the k_{EFF} values seen in Table 2 (to view the extended literature survey of the tropospheric abundances of the co-reactants, see ESI Section S4.2†). As most of these values are averages from single locations across a protracted period of time or a generalised upper-limit in certain urban environments from a variety of locations, most measurements occur over a range of temperatures that include 298 K. Either the k_{THEO} value or the k_{d-d} value are in bold to highlight which the rate constant is used to calculate each k_{EFF} value. Any Γ_{THEO}

© 2023 The Author(s). Published by the Royal Society of Chemistry

Open Access Article. Published on 17 srpna 2023. Downloaded on 07.01.2026 15:12:46.
This article is licensed under a Creative Commons Attribution 3.0 Unported Licence.

Table 2 A tabulation of the reaction kinetics and the atmospheric impact of all HFO-sCI reactions studied here. Characteristics of each reaction listed in table includes co-reactant identity and atmospheric abundance ([co-reactant]); Criegee intermediate labelled by number (sCI); computational master equation rate constant (k_{THEO});[a] dipole–dipole capture limit (k_{d-d}); literature experimental rate constant (k_{EXP}); and effective rate constant ($k_{EFF} = k_{THEO}$ or $k_{d-d} \times$ [co-reactant])[b]

[Co-reactant] (molec. per cm^3)	sCI	k_{THEO} (cm^3 s^{-1})	k_{d-d} (cm^3 s^{-1})	k_{EXP} (cm^3 s^{-1})	k_{EFF} (s^{-1})
HCHO, 2.0×10^{12} (Urban heavy traffic)[128]	**1**	$\mathbf{2.79 \times 10^{-12}}$	1.06×10^{-9}	4.1×10^{-12} (ref. 127)	5.60
	2	$\mathbf{2.69 \times 10^{-13}}$	8.04×10^{-10}	—	0.54
	3	$\mathbf{2.49 \times 10^{-12}}$	6.46×10^{-10}	—	5.0
	4	$\gg k_{d-d}$	$\mathbf{7.20 \times 10^{-10}}$	—	1447
	5	$\mathbf{1.66 \times 10^{-11}}$	7.07×10^{-10}	—	33.4
CF_3CHO	**1**	$\gg k_{d-d}$	6.50×10^{-10}	—	—
CF_3CFO	**1**	$\mathbf{1.98 \times 10^{-12}}$	3.34×10^{-10}	—	—
SO_2, 4.1×10^{11} (Beijing urban area)[129]	**1**	$\gg k_{d-d}$	$\mathbf{7.25 \times 10^{-10}}$	3.9×10^{-11} (ref. 63)	300
	2	$\mathbf{1.90 \times 10^{-12}}$	5.08×10^{-10}	—	0.79
	3	$\gg k_{d-d}$	$\mathbf{4.08 \times 10^{-10}}$	—	169
	4	$\gg k_{d-d}$	$\mathbf{4.51 \times 10^{-10}}$	—	186
	5	$\gg k_{d-d}$	$\mathbf{4.42 \times 10^{-10}}$	—	183
HNO_3, 1.1×10^{11} (Houston, Texas)[130]	**1**	8.22×10^{-9}	$\mathbf{8.45 \times 10^{-10}}$	5.1×10^{-10} (ref. 59)	94
	2	$\mathbf{2.06 \times 10^{-11}}$	5.93×10^{-10}	—	2.3
	3	$\mathbf{8.87 \times 10^{-11}}$	4.76×10^{-10}	—	9.8
	4	9.25×10^{-8}	$\mathbf{5.26 \times 10^{-10}}$	—	58
	5	$\mathbf{7.53 \times 10^{-11}}$	5.16×10^{-10}	—	8.4
TFA, 3.3×10^7 (Beijing higher emission areas)[28]	**1**	$\gg k_{d-d}$	$\mathbf{7.54 \times 10^{-10}}$	3.5×10^{-10} (ref. 61)	2.5×10^{-2}
	2	$\gg k_{d-d}$	$\mathbf{4.96 \times 10^{-10}}$	—	1.7×10^{-2}
	3	$\gg k_{d-d}$	$\mathbf{3.98 \times 10^{-10}}$	—	1.3×10^{-2}
	4	$\gg k_{d-d}$	$\mathbf{4.35 \times 10^{-10}}$	—	1.5×10^{-2}
	5	$\gg k_{d-d}$	$\mathbf{4.27 \times 10^{-10}}$	—	1.4×10^{-2}
H_2O, 6.2×10^{17} (~80% humidity Sao Paulo)[132,133]	**1**	$\mathbf{1.18 \times 10^{-16}}$	1.06×10^{-9}	2.4×10^{-16} (ref. 131)	73
	2	$\mathbf{1.35 \times 10^{-18}}$	8.38×10^{-10}	—	0.83
	3	$\mathbf{1.12 \times 10^{-16}}$	6.73×10^{-10}	—	70
	4	$\mathbf{5.13 \times 10^{-12}}$	7.54×10^{-10}	—	3.2×10^6
	5	$\mathbf{2.27 \times 10^{-13}}$	7.40×10^{-10}	—	1.4×10^5
$(H_2O)_2$, 8.7×10^{14} (~80% humidity Sao Paulo)[132,133]	**1**	$\mathbf{3.28 \times 10^{-12}}$	1.07×10^{-9}	7.5×10^{-12} (ref. 131)	2.9×10^3
	2	$\mathbf{2.71 \times 10^{-12}}$	7.99×10^{-10}	—	2.4×10^3
	3	$\mathbf{3.74 \times 10^{-12}}$	6.42×10^{-10}	—	3.3×10^3
	4	1.14×10^{-6}	$\mathbf{7.14 \times 10^{-10}}$	—	6.2×10^5
	5	1.46×10^{-9}	$\mathbf{7.01 \times 10^{-10}}$	—	6.1×10^5
MeOH, 8.4×10^{11} (Sao Paulo, Brazil)[135]	**1**	$\mathbf{1.20 \times 10^{-14}}$	8.15×10^{-10}	1.1×10^{-13} (ref. 134)	0.010
	2	$\mathbf{9.43 \times 10^{-17}}$	6.14×10^{-10}	—	7.9×10^{-5}
	3	$\mathbf{3.30 \times 10^{-14}}$	4.93×10^{-10}	—	0.028
	4	$\gg k_{d-d}$	$\mathbf{5.50 \times 10^{-10}}$	—	462
	5	$\mathbf{3.31 \times 10^{-11}}$	5.39×10^{-10}	—	28
H_2S, 1.2×10^{13} (industrial landfill)[137]	**1**	$\mathbf{7.06 \times 10^{-15}}$	5.68×10^{-10}	1.7×10^{-13} (ref. 136)	0.052
	2	$\mathbf{1.96 \times 10^{-16}}$	4.26×10^{-10}	—	1.4×10^{-3}
	3	$\mathbf{5.72 \times 10^{-15}}$	3.42×10^{-10}	—	0.042
	4	$\mathbf{6.08 \times 10^{-13}}$	3.81×10^{-10}	—	4.5
	5	$\mathbf{1.23 \times 10^{-14}}$	3.74×10^{-10}	—	0.091
HCl, 1.2×10^{11} (daytime Los Angeles)[138]	**1**	$\mathbf{4.70 \times 10^{-10}}$	6.06×10^{-10}	4.1×10^{-11} (ref. 59)	58
	2	$\mathbf{4.04 \times 10^{-15}}$	4.51×10^{-10}	—	5.0×10^{-3}
	3	$\mathbf{7.28 \times 10^{-11}}$	3.62×10^{-10}	—	8.96
	4	$\mathbf{1.64 \times 10^{-10}}$	4.03×10^{-10}	—	20
	5	$\mathbf{1.13 \times 10^{-10}}$	3.96×10^{-10}	—	14
HF, 3.7×10^{11} (near volcano vicinity ambient T)[139]	**1**	$\mathbf{3.32 \times 10^{-13}}$	8.15×10^{-10}	—	0.12
	2	$\mathbf{6.67 \times 10^{-18}}$	6.14×10^{-10}	—	2.5×10^{-6}
	3	$\mathbf{2.86 \times 10^{-15}}$	4.93×10^{-10}	—	1.1×10^{-3}
	4	$\mathbf{1.19 \times 10^{-11}}$	5.50×10^{-10}	—	4.4
	5	$\mathbf{3.66 \times 10^{-13}}$	5.39×10^{-10}	—	0.14

[a] "$\gg k_{d-d}$" refers to barrierless reactions that yield no k_{THEO} and that the k_{d-d} value should be used instead. [b] In bold is the overall theoretical rate constant, which is the lowest between the k_{THEO} & k_{d-d} values.

branching fractions of the two-step HFO-sCI reactions with aldehydes & SO_2 are not displayed in Table 2 and can be instead found in Sections 3.1 & 3.2.

3.1 HFO-sCI reaction with formaldehyde (HCHO)

During an ozonolysis event that generates a Criegee intermediate, a carbonyl containing species (aldehydes and ketones) are

Open Access Article. Published on 17 srpna 2023. Downloaded on 07.01.2026 15:12:46.
This article is licensed under a Creative Commons Attribution 3.0 Unported Licence.

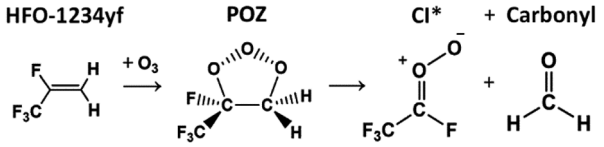

Fig. 3 The general schematic for the ozonolysis of HFO-1234yf producing a short-lived primary ozonide (POZ) followed by one of the pairs of final products, a Criegee intermediate (**sCI 5** or *anti*-CF_3CFOO) and a carbonyl product (formaldehyde).

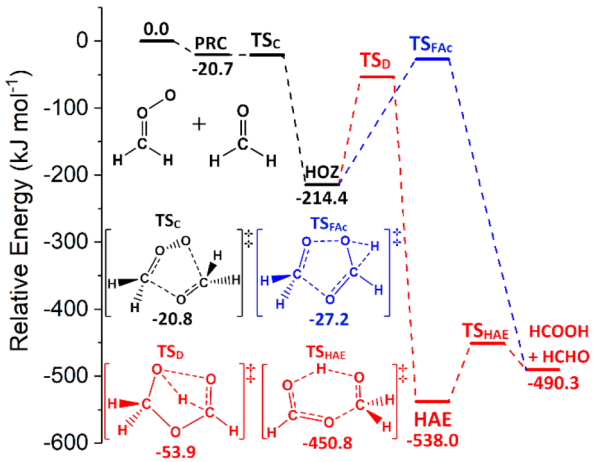

Fig. 4 The potential energy surface for the **sCI 1** + HCHO reaction. The lowest energy transition state for each HOZ fragmentation pathway is displayed. The 1-step direct transfer channel *via* the TS_{FAc} barrier is in blue and a 2-step hydroxyalkyl ester (HAE) channel, *via* the TS_D & TS_{HAE} barriers, is red. Energies are relative to the raw reactants.

very common co-products and as such these carbonyl moieties are co-located with sCIs during formation such that a further reaction between these two proximate species is probable. Formaldehyde (HCHO) is produced from the ozonolysis of a variety of alkenes, notably for this work that includes HFO-1234yf (see Fig. 3), and therefore examining any possible secondary reaction with HCHO is likely vital to understanding the overall tropospheric chemistry of these HFO-sCIs.[4,48,140]

Also, as HCHO emissions are strong in areas of heavy urban traffic (up to 170 μg m^{-3}) and HFOs are used in vehicle coolant units, there is a high probability of emissions overlap between HCHO and HFO-sCIs.[36,128,141,142] Additionally as HCHO is carcinogenic and toxic if inhaled, sCIs depletion of tropospheric HCHO should be included in many atmospheric models.[143–145]

3.1.1 The sCI 1 + HCHO reaction. All sCI + HCHO reactions in this study undergo an initial 1,3-cycloaddition (TS_C) step to a short-lived heteroozonide (HOZ) intermediate and the HOZ almost instantaneously fragments. The fragmentation is likely rapid because the HOZ is formed with significant excess energy and the HOZ structure has a high degree of tortional strain. When the HOZ fragments, it can form acid + aldehyde products *via* two different mechanistic processes: a high energy, 1-step channel or a lower energy, 2-step channel *via* a hydroxyalkyl formate (HAE) species. The schematics and barrier heights of the 1-step "TS_{FAc}" channel (in blue) and the 2-step "HAE channel" (in red) for **sCI 1** + HCHO are seen in Fig. 4. The "TS_D" & "TS_{HAE}" labels are used to refer to the respective formation and breakup of the HAE species.

Computational assessments of the **sCI 1** + HCHO reaction (Fig. 4) are characterised by a low energy TS_C barrier (~−25 to −20 kJ mol^{-1}), which leads to high theoretical rate constants both here ($k_{THEO} \sim 2.79 \times 10^{-11}$ cm^3 s^{-1}) and in the literature ($k_{THEO} \sim 4.03 \times 10^{-10}$ cm^3 s^{-1}).[71,146] The k_{THEO} value determined here is also similar to the k_{EXP} values measured for **sCI 1** + HCHO by Luo *et al.*, $(4.11 \pm 0.25) \times 10^{-12}$, as well as those determined for studies of the analogous **sCI 1** + CH_3CHO reaction (3.0×10^{-13} to 1.7×10^{-12} cm^3 s^{-1}).[64,65,127,147]

The **sCI 1** + HCHO reaction produces only one final product set, HCOOH + HCHO, and of the two HOZ fragmentation mechanism, the TS_D barrier of the two-step HAE channel has a lower energy than the TS_{FAc} barrier to the one-step HOZ fragmentation channel (Fig. 4). Both findings are authenticated by similar results in prior studies.[71,146] Obtaining reliable TS_D & TS_{FAc} barriers is important because whereas the absolute height of the energy barrier(s) of the first reaction step dictates the k_{THEO} value, the crucial factor in determining the Γ_{THEO} branching fractions is the energy difference between the HOZ fragmentation barriers. This study also agrees with other computational studies in that that the second step of the two-step HOZ fragmentation, the breakdown of the HAE, involves a very low TS_{HAE} barrier (Fig. 4).[71,146]

Given that the HAE is formed with considerably higher energy than the HAE → TS_{HAE} barrier height, the MESMER results discussed here are calculated on the assumption that formation of the HAE is the final step of that reaction channel and that all the HAE population reacts further to produce their acid + aldehyde products, with negligible populations of HAE remaining. These MESMER simulations yield a very similar result ($\Gamma_{THEO} \sim 0.973$) to those in which the HCOOH + HCHO are set as the final products ($\Gamma_{THEO} \sim 0.978$). As this methodology has been shown to have little effect on the accuracy, this ~100% HAE → acid + aldehyde conversion principle is applied to the HCHO reactions with **sCIs 2–5**, for the purpose of reducing computational cost.

3.1.2 The HCHO + sCIs 2 & 3 and CF_3CHO + sCI 1 reactions. The cycloaddition of **sCI 2** + HCHO & **sCI 3** + HCHO produce different HOZ conformers, HOZs 1 & 2 respectively, but these HOZ conformers can interconvert *via* an inversion TS_{HOZ} mechanism. This TS_{HOZ} barrier is much lower in energy than both the cycloreversion and HOZ fragmentation mechanisms (Fig. 5). Therefore, these HOZs generally interconvert freely and are treated as a single HOZ species when using MESMER to calculate the product branching fractions. Furthermore, during any of these reactions, (*e.g.* **sCI 2** + HCHO), the HOZ species can fragment to produce any of the other reactant pairs (here **sCI 3** + HCHO or **sCI 1** + CF_3CHO), *via* cycloreversion pathways. The HOZ species produced by these reactions can also fragment (Fig. 5) to produce two different "acid + carbonyl" sets of products, TFA + HCHO or HCOOH + CF_3CHO, either through a one-step channel (*via* TS_{TFA} or TS_{FAc2} respectively) or a two-step HAE channel (*via* TS_{D1} & TS_{HAE1} or TS_{D2} & TS_{HAE2}

© 2023 The Author(s). Published by the Royal Society of Chemistry

Open Access Article. Published on 17 srpna 2023. Downloaded on 07.01.2026 15:12:46.
This article is licensed under a Creative Commons Attribution 3.0 Unported Licence.

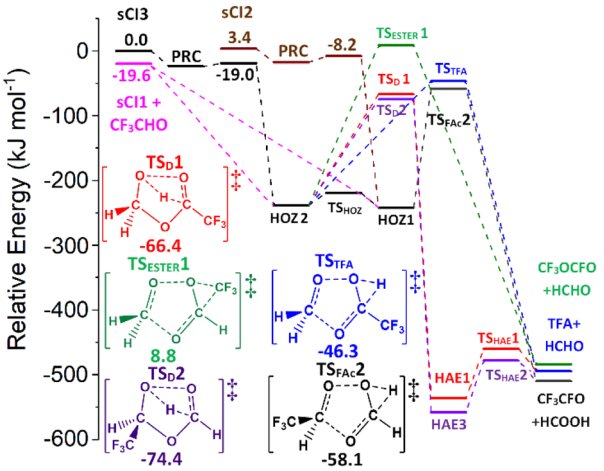

Fig. 5 The collective potential energy surface for **sCIs 2 & 3** + HCHO and **sCI 1** + CF_3CHO reactions with minima energy structures of each HOZ fragmentation displayed. Energies are relative to the raw **sCI 3** + HCHO reactants.

respectively). HOZ fragmentation can also proceed *via* "TS_{ESTER}" mechanisms to produce CF_3OCHO + HCHO.

The relatively low TS_C barriers seen for the **sCIs 2 & 3** reactions with HCHO in Fig. 5, lead to large k_{THEO} values (2.69 & 24.9 × 10^{-13} cm^3 s^{-1}), although both reactions are less reactive than **sCI 1** + HCHO (see Table 3). Studies of the bimolecular HFO-sCI chemistry are limited, but computational work on **sCIs 1–3** reactions with H_2, CO_2 & $CF_3CH{=}CH_2$ are present in the literature and show similar trends to those identified here (Table 3).[72,73,77] For instance, the barriers to the HFO-sCIs + CO_2 reaction follow the same reactivity order (E_{TS} (**sCI 2**) > E_{TS} (**sCI 1**) > E_{TS} (**sCI 3**)) seen for these HCHO reactions.[72] Furthermore, the *anti*-orientated **sCI 3** is more reactive with $CF_3CH{=}CH_2$ than the *syn*-orientated **sCI 2**, the same result observed for **sCIs 2 & 3** + HCHO.[77]

While the inclusion of a single $-CF_3$ group does not significantly enhance the reactivity of **sCIs 2 & 3**, the presence of a single $-CF_3$ substituent in the aldehyde co-reactant increases its reactivity to such a degree that the cycloaddition of **sCI 1** + CF_3CHO is barrierless and the k_{d-d} value (~6.50 × 10^{-10} cm^3 s^{-1}) is used as the rate constant. This could be due to a hypothetical inductive effect caused simply by adding any alkyl substituent to the aldehyde. But, despite the increased number of alkyl groups on CH_3CHO & $(CH_3)_2CO$ the experimental literature suggests that their reactions with **sCI 1** (k_{EXP} ~ 10^{-1}–10^{-12} cm^3 s^{-1}) do not show the enhanced reactivity seen for the **sCI 1** + CF_3CHO reaction.[65,71,147] However, the role of fluorine in $-CF_3$ substituents is explored in an experimental study by Taatjes and co-workers and they show that **sCI 1** + $(CF_3)_2COO$ has a larger k_{EXP} (~3.0 ± 0.3 × 10^{-11} cm^3 s^{-1}) compared to the k_{EXP} of **sCI 1** + $(CH_3)_2COO$ (~2.3 ± 0.3 × 10^{-13} cm^3 s^{-1}).[65] This confirms the high reactivity seen for **sCI 1** + CF_3CHO must emerge from the inductive impact that the fluorenes in the $-CF_3$ substituents have on the aldehyde reactivity.

Both HCHO + **sCI 2** and HCHO + **sCI 3** (Fig. 6) produce high yields of the **sCI 1** + CF_3CHO (~0.91–0.94), due to the barrierless nature of their cycloreversion mechanisms, with small contributions from $\Gamma_{TFA+HCHO}$ (~0.012–0.016) and $\Gamma_{HCOOH+CF_3CHO}$ (~0.052–0.068). In contrast, during the **sCI 1** + CF_3CHO reaction, the production of HCHO + **sCIs 2 & 3** gives very low branching ratios (<0.001) because the energy barriers for producing HCHO + **sCIs 2 & 3** are much larger than other HOZ fragmentation pathways. Consequently, the overall Γ_{THEO} of **sCI 1** + CF_3CHO is dominated by $\Gamma_{HCOOH+CF_3CHO}$ ~ 0.823 with most of this contribution coming from the two-step HAE pathways ($\Gamma_{TS_{D1}}$ ~ 0.746) with a smaller contribution from the one-step channel ($\Gamma_{TS_{FAc}}$ ~ 0.077). The secondary product yield, $\Gamma_{TFA+HCHO}$ ~ 0.177, also has most of its contribution emerge from the two-step HAE pathways, $\Gamma_{TS_{D2}\&TS_{D3}}$ ~ 0.166. The TS_{ESTER} barrier is too high for the ester formation to have anything but a negligible yield for all three reactions.

While no experimental or theoretical product ratios for **sCI 1** + CF_3CHO are available in the literature, some of the analysis of the similar **sCI 1** + CH_3CHO & PhCHO reactions does include computational calculations of HOZ fragmentation energy barriers. Examination of both the **sCI 1** + CH_3CHO & PhCHO systems show patterns consistent with this work, including: that the formation of smaller acid final products was preferred over larger acid products, that the 2-step HAE channel was the favoured formation mechanism for these acids, and that ester formation was negligible.

3.1.3 The HCHO + sCIs 4 & 5 and CF_3CFO + sCI 1 reactions. **sCI 5** + HCHO exhibits has a low energy TS_C barrier (~−28.9 kJ mol^{-1}) whereas the cycloaddition of **sCI 4** + HCHO is barrierless. This demonstrates that **sCI 4** is more reactive than **sCI 5** and that both these HFO-sCIs are significantly more reactive than **sCIs 1–3**. sCIs with larger substituents (*e.g.* $-CH_3$ or $-CF_3$) in the *syn*-position have been shown to decrease sCI reactivity, however here it is observed that **sCI 4**, which has a *syn*-orientated

Table 3 A tabulation of key kinetic information of HCHO reactions with the **sCIs 1–3** reactions from this study contrasted with that other bimolecular **sCIs 1–3** reactions from the literature featuring: the relative energy of the lowest transition state barrier [ΔE_{TS}] and theoretical rate constants [k_{THEO}]. Energies are relative to raw reactants

		ΔE_{TS} [kJ mol^{-1}]				k_{THEO} [10^{-13} cm^3 s^{-1}]	
sCI	#sCI	H_2	CO_2	HCHO	$CF_3CH{=}CH_2$	k_{HCHO}	$k_{CF_3CH=CH_2}$
CH_2OO	**1**	74.5	17.6	−20.8	−12.8	27.9	1.76
Syn-CF_3CHOO	**2**	—	32.6	−11.6	−13.8	2.69	77.9
Anti-CF_3CHOO	**3**	52.3	25.1	−19.0	−16.9	24.9	285
Reference		73	72	This study	77	This study	77

Open Access Article. Published on 17 srpna 2023. Downloaded on 07.01.2026 15:12:46.
This article is licensed under a Creative Commons Attribution 3.0 Unported Licence.

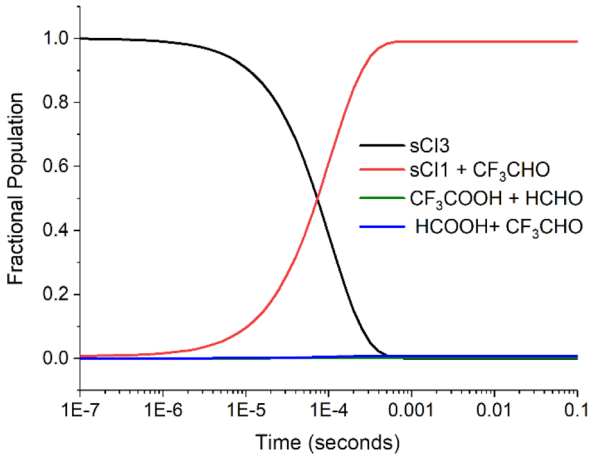

Fig. 6 The fractional populations of reactants and products for the **sCI 3** + HCHO reaction over time (the product branching fractions for the barrierless cycloreversion channels to **sCI 1** + CF_3CHO are calculated using the same reverse ILT method described in the Methods section.[117,124] Excess HCHO reagent concentration is $\sim 1.0 \times 10^{16}$ molec. per cm^3. For other details on the conditions of the reaction see ESI Section S11†).

larger group, has greater reactivity than the *anti*-orientated **sCI 5**.[60,79,148–151] Unlike the **sCI 1** + CF_3CHO reaction, **sCI 1** + CF_3CFO does not have barrierless cycloaddition (TS_C ~ -27 to -22 kJ mol^{-1}) and the k_{THEO} value of this reaction ($\sim 2.0 \times 10^{-12}$ cm^3 s^{-1}) is below the k_{d-d} capture limit. When compared to the k_{THEO} values of **sCI 1** + HCHO & CF_3CHO (~ 2.8 & 650×10^{-12} cm^3 s^{-1}), it is clear that the inductive effect of the $-CF_3$ substituent in the CF_3CFO is largely cancelled out by the larger deactivating effect of the –F substituent that is also present in CF_3CFO.

sCI 4 & **sCI 5** reactions with HCHO are both integrated into the same reaction system as **sCI 1** + CF_3CFO and therefore all sCI + aldehyde reactant pairs can also be produced during HOZ fragmentation in this overall reaction system. The Γ_{THEO} for both the **sCIs 4** & **5** + HCHO reactions are dominated by yields of **sCI 1** + CF_3CFO (~ 0.84) with the remainder being the $\Gamma_{HCOOH+CF_3CFO}$ contribution (~ 0.16). In contrast, the **sCI 1** + CF_3CFO reaction has only negligible yields for **sCIs 4** & **5** + HCHO (<0.0001) because their cycloreversion TS_C barriers are >100 kJ mol^{-1} higher than the lower energy HOZ fragmentation barriers.

The primary product of the **sCI 1** + CF_3CFO reaction is HCOOH + CF_3CFO ($\Gamma_{HCOOH+CF_3CFO} > 0.99$), with the direct H-transfer TS_{FAc} channel producing almost all the formic acid yield. The higher barriers to the HAE pathway compared to the direct H-transfer channel seen here for the **sCI 1** + CF_3CFO reaction system (see ESI Section S5†) is uncommon both in this study and in the literature.[71,146] However, in a literature analysis of *anti*-PhCHOO + PhCHO, the direct H-transfer mechanism also has a higher barrier (-19.2 kJ mol^{-1}) to phenylacetic acid formation than the two step HAE channel (-17.6 kJ mol^{-1}).[146] As noted in Table 4, ester formation continues to be negligible for all sCI + aldehyde reactions.

3.1.4 Overview of sCI + aldehyde reactions. The key features of the sCI + aldehyde reactions are that the chemistry can be broadly divided into two steps: the cycloaddition into an HOZ intermediate, and the fragmentation of that intermediate into various products. The HFO-sCI + aldehyde reactions have large rate constants ($k_{THEO} \sim 10^{-13}$–10^{-10} cm^3 s^{-1}) as the cycloaddition is either barrierless or proceeds *via* low energy TS_C barriers. The inclusion of $-CF_3$ substituents in the *syn*-position produces a reductive impact on the COO group of the sCI, as shown by the smaller rate constant of **sCI 2** compared to the unsubstituted **sCI 1** or the *anti*-substituted **sCI 3**. However, an –F substituent has an inductive effect on the sCI, particularly in the *anti*-position, as shown by the high reactivity of **sCI 4**. Considering the factors given above the reactivity of the HFO-sCIs studied here follows the following trend: k_{THEO} (**sCI 2**) < k_{THEO} (**sCI 3**) < k_{THEO} (**sCI 1**) < k_{THEO} (**sCI 5**) < k_{d-d} (**sCI 4**). The role these –H, –F or $-CF_3$ substituents have on the aldehyde reactivity trend, k_{THEO} (**CF_3CFO**) < k_{THEO} (**HCHO**) < k_{THEO} (**CF_3CHO**), is the opposite to that seen for the sCIs, k_{THEO} (**CF_3CFOO**) < k_{THEO} (**CH_2OO**) < k_{THEO} (**CF_3CHOO**). In the HOZ fragmentation stage of the **sCI 1** + HCHO/CF_3CHO/CF_3CFO reactions, the yield is dominated by formation of formic acid + an aldehyde, with **sCI 1** + CF_3CHO also producing sizable product branching fractions for HCHO + CF_3-COOH ($\Gamma_{THEO} \sim 0.16$). However, for **sCIs 2–5** + HCHO reactions, the dominant product is **sCI 1** + CF_3CHO/CF_3CFO ($\Gamma_{THEO} \sim 0.80$–0.99), due to the low barrier to formation of this product pair.

Table 4 A tabulated breakdown of the results from the HOZ fragmentation of all HFO-sCI + aldehyde & ketone studied here, giving the final product branching for each product set

	Final product branching ratio (Γ_{THEO})				
Reaction sCI + HCHO	$\Gamma_{sCI1+R_1CR_2O}$	$\Gamma_{HCHO+R_1CR_2OO}$	$\Gamma_{HCOOH+R_1CR_2O}$	$\Gamma_{TFA+HCHO}$	$\Gamma_{ester+HCHO}$
sCI 2 + HCHO	0.993[a]	7.40×10^{-5}	0.006	0.001	1.78×10^{-7}
sCI 3 + HCHO	0.991[a]	3.92×10^{-6}	0.007	0.002	1.02×10^{-7}
sCI 4 + HCHO	0.843	9.40×10^{-9}	0.156	—	3.06×10^{-5}
sCI 5 + HCHO	0.842	8.13×10^{-9}[a]	0.158	—	4.98×10^{-5}
sCI 1 + R_1CR_2O	$\Gamma_{HCHO+anti\text{-}R_1CR_2OO}$	$\Gamma_{HCHO+syn\text{-}R_1CR_2OO}$	$\Gamma_{HCOOH+R_1CR_2O}$	$\Gamma_{TFA+HCHO}$	$\Gamma_{ester+HCHO}$
sCI 1 + CF_3CHO	1.47×10^{-6}	2.49×10^{-5}	0.823	0.177	2.14×10^{-8}
sCI 1 + CF_3CFO	3.10×10^{-14}	3.51×10^{-12}[a]	>0.999	—	1.74×10^{-7}

[a] The product branching fractions of the barrierless cycloreversion channels that leads to either **sCI 1** + CF_3CHO or **sCI 4** + HCHO are calculated using the same reverse ILT method described in Method section.[117,124]

© 2023 The Author(s). Published by the Royal Society of Chemistry

Open Access Article. Published on 17 srpna 2023. Downloaded on 07.01.2026 15:12:46.
This article is licensed under a Creative Commons Attribution 3.0 Unported Licence.

3.2 HFO-sCIs reactions with sulphur dioxide (SO_2)

Toxic sulphur dioxide (SO_2) emitted from various sources, including the burning of fossil fuels and volcanic eruptions, has a major role as an effective gaseous sCI sink and the sCI + SO_2 reaction is therefore of significant prominence in the literature.[63,78,81,82,84,85,131,149,152–158] This reaction is considered responsible for between ~1% of the loss of *syn*-CH_3CHOO in rural environments to ~22% of the loss of "*syn*-CH_3-*anti*-(*trans*-CH_2=CH)–COO" in boreal forests.[159] Furthermore, the importance of this reaction is increased because the dominant final product of this reaction is SO_3, which is a source of organosulphates and is involved in the formation and growth of secondary organic aerosol (SOA) nuclei.[84,85,160] The promotion of SOA nucleation, caused by increased SO_3 yields, is vital to understand because the prevalence of aerosols in urban environments can cause serious respiratory problems and premature death.[161–165] Also, depending on the aerosol type, they can absorb and scatter solar radiation and therefore influence climate temperatures.[161,164,165]

3.2.1 The sCI 1 + SO_2 reaction. All HFO-sCIs in this study, as well as many sCIs studied in the literature, react with SO_2 through a general two-step reaction scheme, *via* a short-lived 5-member ozonide ring.[84,159] These pathways produce cyclic intermediates, which are often called heteroozonides too, but it can also be referred to as a secondary ozonide (SOZ) and to prevent confusion with the HCHO reaction, that SOZ label is used in these SO_2 reactions.[84] The SOZs produced from **sCI 1** + SO_2 are generated in either an *exo*- (SOZ 1) or an *endo*- orientation (SOZ 2), depending on the orientation of the SO_2 (Fig. 7) in the cycloaddition transition state, TS_{EXO} and TS_{ENDO} respectively. As also observed in the experimental and theoretical literature, the **sCI 1** + SO_2 reaction is highly reactive and so when both TS_{ENDO} and TS_{EXO} pathways were evaluated it was found that both reactions were barrierless.[63,64,84,85,153,154,166] This meant that therefore means that the k_{d-d} limit (7.25×10^{-10} cm^3 s^{-1}) is adopted as the rate constant for the **sCI 1** + SO_2 reaction.

The SOZ interconversion *via* the inversion of the S atom is known to require >180 kJ mol^{-1} excess energy, which exceeds barriers to both cycloreversion (*via* TS_{EXO} & TS_{ENDO}) and SOZ fragmentation (Fig. 8).[84] This would impede SOZ interconversion but, as the R_1 and R_2 substituents in **sCI 1** are identical, SOZs 1 & 2 can freely interconvert over low energy pseudorotation TS_{SOZ} barriers (see Fig. 8), which this means that SOZs 1 & 2 behaves as a single SOZ species.

The next stage of the **sCI 1** + SO_2 reaction is the fragmentation of the SOZ to produce either SO_3 + HCHO *via* the TS_{SO_3} channel or SO_2 + HCOOH *via* the TS_{acid} channel. All SOZ fragmentation channels studied here are single-step mechanisms and the acid-producing mechanisms from each HFO-sCI + SO_2 reaction system exclusively produces a single acid species. Kuwett *et al.* have performed a comprehensive analysis of both SO_2 reactions with **sCIs 1** & $(CH_3)_2COO$ comprising a numerous range of major and minor SOZ fragmentation pathways, including a homolytic O–O bond fission to produce a 1,5-(bis) oxy diradical intermediate product.[84] While the self-reaction of this diradical intermediate produces important products, such as SOCO rings, sulphurous anhydrides or 1,3-(bis)oxy diradicals, its yield is so minor that 1,5-(bis)oxy diradical pathways are not explored for **sCIs 1–5** + SO_2 here.[84]

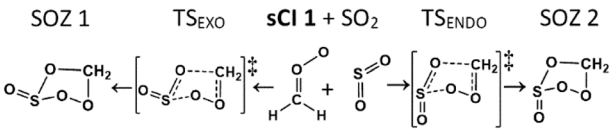

Fig. 7 A Schematic of the cycloaddition process for **sCI 1** + SO_2: featuring the *endo*- & *exo*-cycloaddition transition states (TS_{EXO} & TS_{ENDO}) and the *endo*- & *exo*-SOZ intermediate products (SOZs 1 & 2).

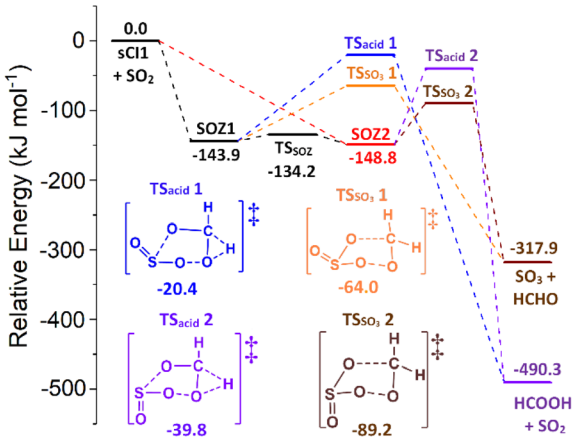

Fig. 8 The potential energy surface of **sCI 1** + SO_2 with minima energy structures of each SOZ fragmentation displayed. Energies are relative to the raw reactants.

The final product branching fraction for **sCI 1** + SO_2 is dominated by SO_3 + HCHO ($\Gamma_{SO_3} \sim 0.966$) with a subordinate yield HCOOH + SO_2 ($\Gamma_{acid} \sim 0.034$) because the TS_{SO_3} 1 & 2 barriers (Fig. 8) are significantly lower in energy than the TS_{acid} 1 & 2 structures. This dominance of SO_3 + CF_3CHO in the Γ_{THEO} value is in agreement with that calculated in the literature ($\Gamma_{SO_3} \sim 0.973$–0.984).[84]

3.2.2 The sCIs 2 & 3 + SO_2 reactions. The **sCI 2** + SO_2 reaction is unique amongst the HFO-sCI + SO_2 reactions studied here in that the cycloaddition process is not barrierless and structures for the TS_{ENDO} & TS_{EXO} barriers can be readily computationally determined. The TS_{ENDO} barrier (−18.3 kJ mol^{-1}) is lower in energy than TS_{EXO} (−17.6 kJ mol^{-1}) and so the *endo*-orientated SOZ 2 yield is greater than *exo*-orientated SOZ 1 at a ratio of 0.69 : 0.31. Even though all other SO_2 reactions with **sCIs 1–5** are barrierless, **sCI 2** + SO_2 still has a substantially large theoretical rate constant ($k_{THEO} = 1.90 \times 10^{-12}$ cm^3 s^{-1}). As both the TS_{EXO} & TS_{ENDO} channels of **sCI 3** + SO_2 are barrierless, the k_{d-d} value (4.08×10^{-10} cm^3 s^{-1}) is assigned as the rate constant and SOZs 3 & 4 are produced in equal fractions.

Due to the high energy barrier for interconversion *via* inversion of the S atom (>180 kJ mol^{-1}), the SOZ 1 & 2 conformers, produced from the SO_2 reaction with the mono-substituted **sCI 2**, cannot interconvert with each other without

Open Access Article. Published on 17 srpna 2023. Downloaded on 07.01.2026 15:12:46.
This article is licensed under a Creative Commons Attribution 3.0 Unported Licence.

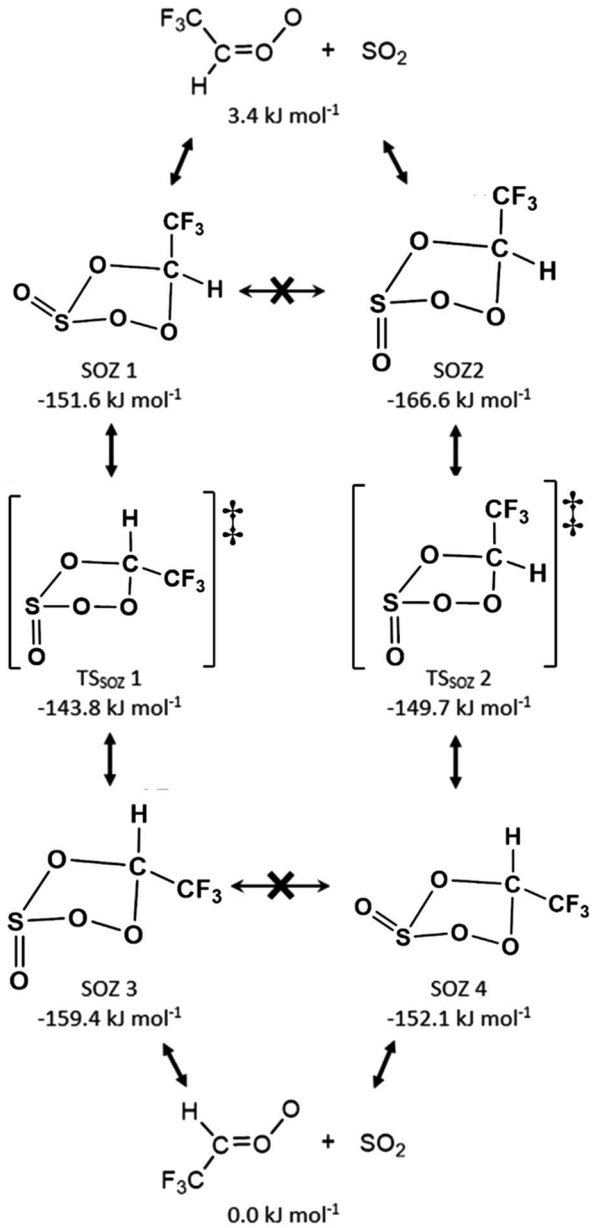

Fig. 9 Collective diagram of all SOZs produced by **sCIs 2** & **3** + SO_2 reactions and the pseudorotation TS_{SOZ} barriers that facilitate SOZ 1 ↔ SOZ 3 and SOZ 2 ↔ SOZ 4 interconversions. Structures included and energies relative to **sCI 3** + SO_2.

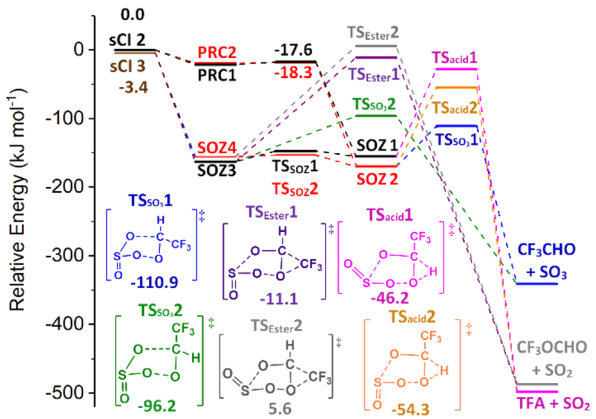

Fig. 10 The collective potential energy surface for **sCIs 2** & **3** + SO_2 reactions with minima energy structures of each SOZ fragmentation displayed. Energies are relative to the raw **sCI 2** + SO_2 reactants.

reverting to the initial reactants. This likewise applies to the mono-substituted **sCI 3** + SO_2, which also produces *endo* and *exo* conformers SOZs 3 & 4. During some sCI + SO_2 reactions, the SOZs produced can interconvert *via* a pseudorotation TS_{SOZ} mechanism and circumvent the higher barrier *via* S atom inversion, but this can only transpire during reactions with sCIs with the same R_1 & R_2 substituents (*e.g.* **sCI 1** or $(CH_3)_2COO$). Instead, when SOZ 1 surmounts the pseudorotation TS_{SOZ} 1 barrier it isomerises into the SOZ 3 conformer and the TS_{SOZ} 2 pseudorotation makes possible the SOZ 2 ↔ SOZ 4 interconversion (Fig. 9). This also means that SO_2 reactions with **sCIs 2** & **3** are part of the same integrated PES, through the TS_{SOZ} 1 & 2 isomerisation channels (Fig. 9 and 10). This phenomena of 2 × non-interchangeable sets of SOZs also applies to SO_2 reactions with **sCIs 4** & **5** and, according to the literature, SO_2 reactions with *syn*- & *anti*-CH_3CHOO.[84]

During the SOZ fragmentation of either **sCI 2** + SO_2 & **sCI 3** + SO_2 reactions, the reverse sCI + SO_2 reactant pairs can be produced through cycloreversion, as both reactions are part of the same potential energy surface. The SOZ fragmentation can also proceed through: TS_{SO_3} into SO_3 + CF_3CHO, TS_{acid} into SO_2 + TFA, or TS_{Ester} into SO_2 + CF_3OCHO. It was noted above that the cycloaddition step of the SO_2 + **sCI 2** reaction produced a large yield of the SOZ 2 & 4 conformer set and a small yield of the SOZ 1 & 3 conformer set, whereas the SO_2 + **sCI 3** produced fairly even yields of each SOZ set. Furthermore, these stereochemically distinct SOZ sets each have their own fragmentation pathways, as SOZ 1 & 3 breakdown *via* TS_{SO_3} 2, TS_{acid} 1 & TS_{Ester} 1 and SOZ 2 & 4 fragments *via* TS_{SO_3} 1, TS_{acid} 2 & TS_{Ester} 2. The overall product branching ratio for **sCI 2** + SO_2 is very similar to that of **sCI 3** + SO_2, so it appears that the differing SOZ yields seen in these two reactions has little overall effect on the product branching fraction.

sCI 2 + SO_2 does produce a small yield of **sCI 3** + SO_2 from the cycloreversion channel, whereas the **sCI 2** + SO_2 yield from **sCI 3** + SO_2 reaction is negligible. This is because cycloreversion to **sCI 2** + SO_2 has to overcome TS barriers, whereas cycloreversion to **sCI 3** + SO_2 only has to overcome the energy of required to reform the raw reactants. The product branching fraction for ester formation is slight. The dominant final products for both the **sCIs 2** & **3** + SO_2 reactions are CF_3CHO + SO_3 ($\Gamma_{THEO} \sim 0.995$) with only a very minor yield of TFA + SO_2 ($\Gamma_{THEO} \sim 0.003$).

3.2.3 sCIs 4 & 5 + SO_2 reactions. Both SO_2 reactions with **sCIs 4** & **5** are barrierless, so their k_{d-d} values (4.51 & 4.42 × 10^{-10} cm^3 s^{-1}) are used for the rate constants for these reactions and their *exo*- & *endo*-SOZ conformers are produced in almost equal yields. The **sCIs 4** & **5** + SO_2 reactions are part of the same integrated reaction system and the phenomenon of 2 sets of non-interchangeable SOZs also applies to this system (Fig. 11) but this has little impact on SOZ fragmentation yields (Table 5).

© 2023 The Author(s). Published by the Royal Society of Chemistry

Open Access Article. Published on 17 srpna 2023. Downloaded on 07.01.2026 15:12:46.
This article is licensed under a Creative Commons Attribution 3.0 Unported Licence.

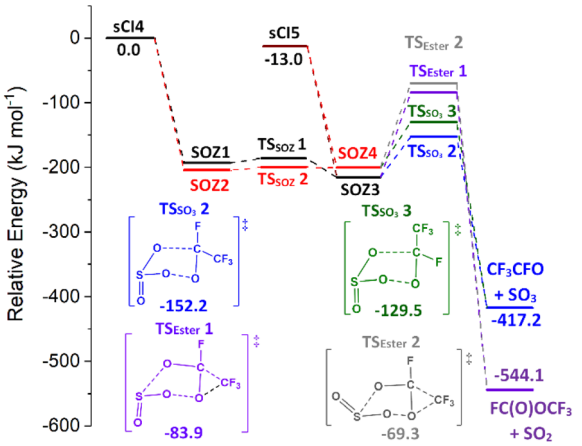

Fig. 11 The collective potential energy surface for **sCIs 4** & **5** + SO_2 reactions with minima energy structures of each SOZ fragmentation displayed. Energies are relative to the raw **sCI 4** + SO_2 reactants.

The only other SOZ fragmentation calculated here are TS_{SO_3} & TS_{ESTER} channels, as an SOZ → acid channel cannot transpire from SO_2 reactions with **sCIs 4** & **5** (Fig. 11). The cycloreversion channel has a negligible yield in the **sCI 5** + SO_2 reaction and a minor role in **sCI 4** + SO_2 reaction (Table 5). While TS_{ESTER} 1 & 2 are not extremely high in energy, the ester yield is still small ($\Gamma_{SO_2+CF_3OCHO} \sim 0.01$). The low TS_{SO_3} barriers and the minor yields of other products means that the predominant products from SOZ fragmentation are SO_3 + CF_3CHO (~0.986 & 0.996).

3.2.4 Overview of sCI + SO_2 reactions. There are several key results from this analysis of the HFO-sCI + SO_2 reactions, including that all these reactions are initiated *via* a cycloaddition generating a short-lived SOZ ring, that then fragmented. **sCI 2** + SO_2 was the only reaction without a barrierless cycloaddition step, which confirms that the *syn*-orientated **sCI 2** is less reactive than the *anti*-orientated **sCI 3**. This contributes to producing an HFO-sCI + SO_2 general reactivity trend of: k_{THEO} (**sCI 2**) < k_{d-d} (**sCI 3**) < k_{d-d} (**sCI 5**) < k_{d-d} (**sCI 4**) < k_{d-d} (**sCI 1**). Lastly, the most dominant products of these reactions were SO_3 + aldehydes ($\Gamma_{SO_3+aldehyde} \sim 0.96$–$0.99$) with only small yields of either acids, esters or other sCIs. This implies that emissions of the HFO-sCIs will lead to consequentially higher local concentrations of SO_3 and subsequently higher concentrations of atmospheric aerosols.

3.3 HFO-sCIs reactions with organic and inorganic acids

Both organic acids such as TFA & carboxylic acids, and inorganic acids including HNO_3 & HCl, are prevalent in various tropospheric environments (see ESI Section S4.2† for more details) and sCIs is their capacity to deplete these acids.[49,59,77,130,138,139,167]

3.3.1 HFO-sCI reactions with HNO_3. The sCI + HNO_3 reaction almost exclusively forms a nitrooxyalkyl hydroperoxide (NAHP) species by reacting *via* a 1,4-insertion mechanism, such as that seen in Fig. 12. In previous studies of **sCI 1** + HNO_3 the chemistry of NAHP fragmentation was also calculated, but as this process occurs over a long timescale, NAHP breakdown is beyond the scope of this study. In contrast, the HOZ/SOZ fragmentation in the sCI + HCHO or SO_2 reactions occurs almost instantaneously.[168,169] NAHP can also be produced *via* a 1,2-insertion mechanism, but it has been excluded from this study as this barrier is ~30 kJ mol^{-1} greater in energy than the 1,4-insertion barrier.[169]

None of the 1,4-insertion processes for HFO-sCI + HNO_3 reactions studied here are barrierless, but the high reactivity of **sCI 1** + HNO_3 means that the k_{THEO} value (8.21×10^{-9} cm^3 s^{-1}) is so great that the k_{d-d} limit (8.45×10^{-10} cm^3 s^{-1}) is used as the rate constant instead. This k_{d-d} limit is also similar to the k_{EXP} [295 K] value (5.4×10^{-10} cm^3 s^{-1}) from the experimental Foreman *et al.* study.[59]

The trend in reactivity indicated by these HFO-sCI + HNO_3 relative barrier heights, ΔE_{TS} (**sCI 2**) > ΔE_{TS} (**sCI 3**) > ΔE_{TS} (**sCI 1**) > ΔE_{TS} (**sCI 5**) > ΔE_{TS} (**sCI 4**), further verifies the HFO-sCI reactivity series seen in previous sections. However, the overall reactivity trend, k_{THEO} (**sCI 2**) < k_{THEO} (**sCI 3**) < k_{THEO} (**sCI 5**) < k_{d-d} (**sCI 4**) < k_{d-d} (**sCI 1**), is altered by the rate constants of HNO_3 reactions with **sCIs 1** & **4**, which reaching the k_{d-d} limit, and an surprisingly low k_{THEO} value for **sCI 5** + HNO_3 (7.57×10^{-11} cm^3 s^{-1}).

3.3.2 HFO-sCI reactions with TFA. In general, **sCIs 1–5** react with TFA to produce a hydroperoxy ester (HPE) species through a barrierless minimum energy pathway (*e.g.* Fig. 13).

Table 5 A tabulated breakdown of the outcomes from SOZ fragmentation of the **sCIs 1–5** + SO_2 reactions studied here, giving the final product branching for each product set

		Product branching ratio (Γ_{THEO})			
Reaction	sCI#	$\Gamma_{SO_3+aldehyde}$	Γ_{SO_2+acid}	$\Gamma_{SO_2+ester}$	$\Gamma_{SO_2+other\ CI}$
CH_2OO + SO_2	**1**	0.968	0.032	N/A	N/A
Syn-CF_3CHOO + SO_2	**2**	0.9922	0.0019	<0.0001	SO_2 + **sCI3:** 0.0059[a]
Anti-CF_3CHOO + SO_2	**3**	0.9973	0.0027	<0.0001	SO_2 + **sCI2:** <0.0001
Syn-CF_3CFOO + SO_2	**4**	0.9860	N/A	0.0090	SO_2 + **sCI5:** 0.0050[a]
Anti-CF_3CFOO + SO_2	**5**	0.9955	N/A	0.0045	SO_2 + **sCI4:** <0.0001[a]

[a] The product branching fractions of the barrierless cycloreversion channels that lead to SO_2 + **sCIs 3**, **4** or **5** are calculated using the same reverse ILT method described in Method section.[117,124]

Open Access Article. Published on 17 srpna 2023. Downloaded on 07.01.2026 15:12:46.
This article is licensed under a Creative Commons Attribution 3.0 Unported Licence.

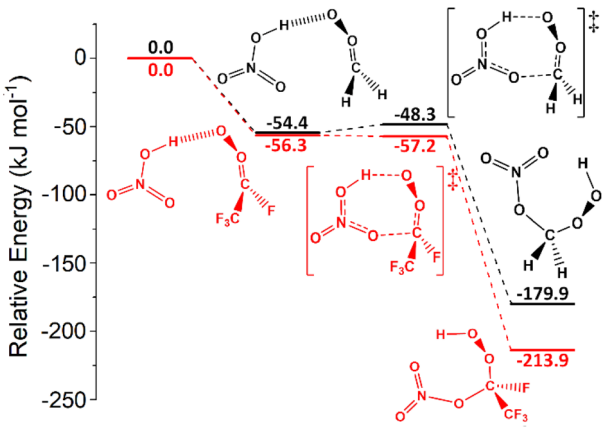

Fig. 12 The potential energy surfaces for the **sCI 1** + HNO_3 (black) and **sCI 4** + HNO_3 (red) reactions. Energies are relative to raw reactants.

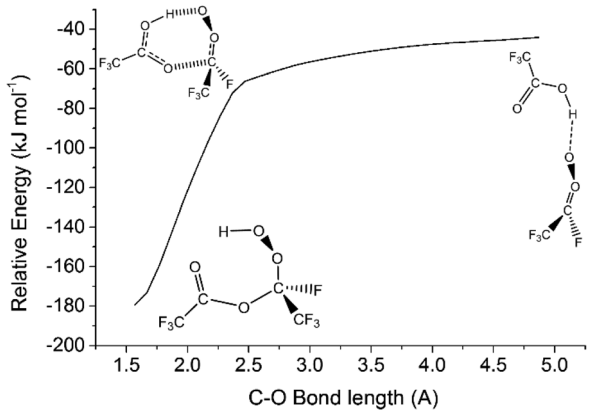

Fig. 13 The barrierless minimum energy pathway for the **sCI 4** + TFA reaction. Energies displayed here are derived from using the B3LYP/aug-cc-pVTZ approach. Energies displayed here are relative to raw reactants.

The barrierless minimum energy pathway calculated here for **sCI 1** + TFA is similar to literature schemes and its k_{d-d} capture limit (7.54×10^{-10} cm^3 s^{-1}) is found to be in close proximity to the k_{EXP} rate constant (3.4×10^{-10} cm^3 s^{-1}).[61]

Altering the sCI substituents does not alter the barrierless nature of the HFO-sCI + TFA reaction profiles studied here (see ESI Section S8.5†). For this reason, all the **sCIs 1–5** + TFA reactions use the k_{d-d} values as rate constants ($3.98–7.54 \times 10^{-10}$ cm^3 s^{-1}).

3.4 HFO-sCI reactions with water monomer and dimer

Due to the high tropospheric concentration of water vapour, water acts as the most prevalent bimolecular sink for sCIs, and therefore examining the chemistry of **sCIs 1–5** reactions with H_2O & $(H_2O)_2$ is essential. **sCIs 1–5** reactions with H_2O proceed through only two reaction channels (TS_{H_2O} 1 and TS_{H_2O} 2), whereas **sCIs 1–5** reactions with $(H_2O)_2$ proceed *via* four pathways: $TS(H_2O)_2$ 1, $TS(H_2O)_2$ 2, $TS(H_2O)_2$ 3 and $TS(H_2O)_2$ 4 (see ESI Section S8.9†). One commonality between these reactions is that the primary product is an α-hydroxy-hydroperoxide (HHP), which is implicated in both forest damage and generating crucial secondary products (inc. H_2O_2, organic acids & aldehydes).[86,170–176]

As the yields of the HHP products are sizable, the atmospheric fate of these HHPs is the subject of many scientific studies.[67,68,131,150,157,177–179] Under standard conditions, photolysis, deposition, and reaction with hydroxyl radicals are usually the main sinks for HHPs, but the excess internal energy within the HHP at the point of formation increases the significance of thermal unimolecular HHP decay.[131,177] The primary unimolecular decay mechanism for hydroxymethyl hydroperoxide (HMHP), the product of CH_2OO + H_2O, is the elimination of H_2O_2 to produce formaldehyde, with some yields from minor channels that produce either H_2O + HCOOH or OH + OCH_2OH.[180,181] Sheps *et al.* showed in a study of CH_2OO + $(H_2O)_2$ that while ~55% of the HMHP remained stable, this excess energy led to ~40% of the HMHP fragmenting to produce H_2O_2 and formaldehyde, both of which are implicated in biogenic degradation.[131] Halogenated HHPs produced from **sCIs 2–5** are also likely to be produced with excess energy, and therefore exploring the breakdown of these products may be useful in the future.

The k_{THEO} value produced for **sCI 1** + H_2O (1.18×10^{-16} cm^3 s^{-1}) is within the range of literature k_{EXP} values ($0.25–13 \times 10^{-16}$ cm^3 s^{-1}), and is particularly close to the rate constant found by Sheps *et al.* (k_{EXP} [293 K, 50 Torr] ~ 2.4×10^{-16} cm^3 s^{-1}).[64,78,131,182,183] Furthermore, both the k_{THEO} value in this study and the k_{EXP} value found in the literature agree that **sCI 1** + H_2O reactions slower than **sCI 1** reactions with HNO_3, SO_2 or TFA.[59,61,63,64,85,153,154,166]

The computational rate constants of the **sCIs 4** & **5** + H_2O reactions were found to have a negative temperature dependence, where 200 K < T < 400 K, whereas **sCIs 1**, **2** & **3** + H_2O all have a positive temperature dependence within the same range (see ESI Section 1.2†). The general reactivity trend for these sCI + H_2O reactions continues the trend observed throughout most of this study k_{THEO} (**sCI 2**) < k_{THEO} (**sCI 3**) ≤ k_{THEO} (**sCI 1**) < k_{THEO} (**sCI 5**) < k_{THEO} (**sCI 4**). The theoretical trend of **sCI 4** being more reactive than **sCI 5** is partially obscured by rate constants being near to or exceeding the k_{d-d} limit, however as neither the k_{THEO} values for **sCI 4** + H_2O (5.13×10^{-12} cm^3 s^{-1}) or **sCI 5** + H_2O (2.27×10^{-13} cm^3 s^{-1}) reach the k_{d-d} limit, sCI + H_2O would provide an experimental case study to verify if k_{THEO} (**sCI 4**) does exceed k_{THEO} (**sCI 5**) in bimolecular reactions.

In contrast, HFO-sCI + $(H_2O)_2$ reactions are faster as a result of **sCI 5** + $(H_2O)_2$ having a lower reaction barrier than **sCI 5** + H_2O (Fig. 14). The greater reactivity of sCI + $(H_2O)_2$ reactions is evidenced by k_{EXP} values found for **sCI 1** + $(H_2O)_2$ ($4.0–8.2 \times 10^{-12}$ cm^3 s^{-1}), which are in close proximity to the large k_{THEO} value calculated here (3.28×10^{-12} cm^3 s^{-1}).[78,131,156–158,184] In line with previous HFO-sCI reactions, **sCI 2** + $(H_2O)_2$ has the lowest k_{THEO} value (2.71×10^{-12} cm^3 s^{-1}) but unusually the **sCI 3** reaction with $(H_2O)_2$ has a greater k_{THEO} value (3.74×10^{-12} cm^3 s^{-1}) than **sCI 1**. None of the 4 × $TS(H_2O)_2$ channels for H_2O reactions with either **sCI 4** or **sCI 5** are barrierless, but the very high reactivity of these reactions leads to very large k_{THEO} values (1.14×10^{-6} & 1.46×10^{-9} cm^3 s^{-1}). This means that the k_{d-d}-constants of **sCIs 4** & **5** + H_2O (~7×10^{-10} cm^3 s^{-1}) are used as

© 2023 The Author(s). Published by the Royal Society of Chemistry

Open Access Article. Published on 17 srpna 2023. Downloaded on 07.01.2026 15:12:46.
This article is licensed under a Creative Commons Attribution 3.0 Unported Licence.

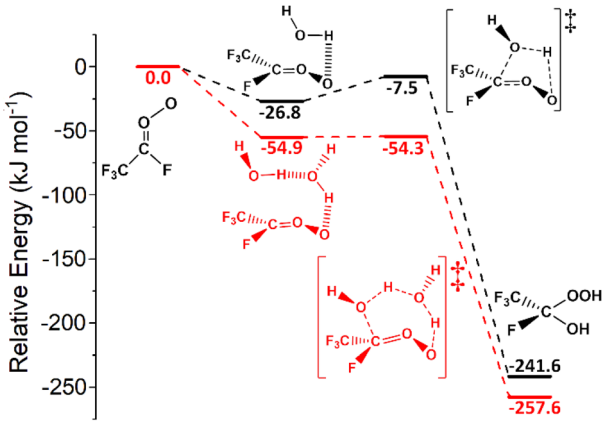

Fig. 14 The potential energy surfaces for the **sCI 5** + H_2O (in black) and **sCI 5** + $(H_2O)_2$ (in red) reactions. Energies are relative to raw reactants.

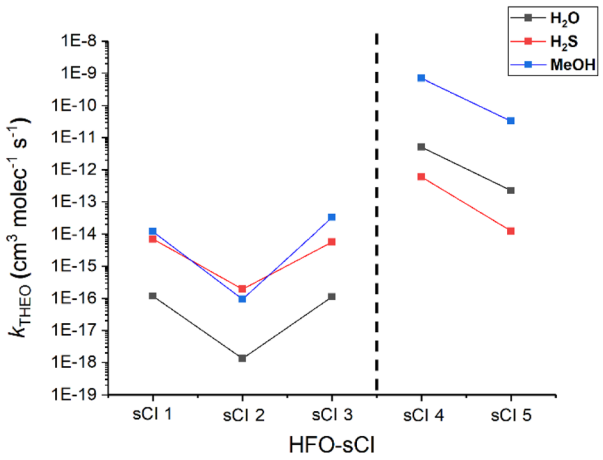

Fig. 15 A comparison of the impact that heteroatom tuning of the group XVI-centred co-reactant (identity in the legend) has on the bimolecular rate constant (k_{THEO}) of different HFO-sCI reaction. Of note in this figure is the large increase in reactivity for **sCIs 4 & 5** + H_2O and MeOH that is not observed for H_2S reactions.

the rate constants instead. Overall the reactivity trend for HFO-sCI + $(H_2O)_2$ reactions: k_{THEO} (**sCI 2**) < k_{THEO} (**sCI 1**) ≈ k_{THEO} (**sCI 3**) < k_{d-d} (**sCI 5**) ≈ k_{d-d} (**sCI 4**).

Criegee intermediates exhibit a mixed biradical and zwitterionic character and it has been shown that the more reactive zwitterionic dominated COO moieties have the larger ratio of OO and CO bond lengths, R_{OO}/R_{CO} or q.[68,74] Given these observations, **sCIs 2 & 3** (q = 1.064 & 1.071) appear to have a more biradical COO moiety than **sCI 1** (q = 1.078), whereas **sCIs 5 & 4** (q = 1.101 & 1.114) are more zwitterionic. Anglada *et al.* noted in a computational study of sCI + H_2O reactions that the degree of this zwitterionic nature of the carbonyl oxide moiety, and consequentially it's reactivity, can be tuned by modification of the substituents.[68] Furthermore, in a computational study of sCI + alcohol reactions it is noted that the electron-withdrawing nature of F substituents in *syn-* & *anti*-FCHOO is likely to increase the unsaturated nature of the zwitterionic carbonyl oxide. This then generates a more electropositive central C atom, which is more vulnerable to nucleophilic attack by the alcohol's electronegative O atom. This study shows the same positive relationship between electron-withdrawing groups, zwitterionic COO moiety and high reactivity seen in the literature, as shown by the fact that increases in q values in the HFO-sCI series mostly correlates with the growth in rate constant: k_{THEO} (**sCI 2**) < k_{THEO} (**sCI 3**) ≈ k_{THEO} (**sCI 1**) < k_{THEO} (**sCI 5**) < k_{THEO} (**sCI 4**).

3.5 Impact of heteroatom tuning on HFO-sCI reactions

It has been suggested that for sCI + H_2X (X = O, Si, Se & Te) reactions, as the central X atom in the H_2X co-reactant is substituted with larger group XVI elements, the rate constant increases.[87] In this section, the computational analysis of the **sCIs 1–5** + H_2S reactions is compared with **sCIs 1–5** reactions with H_2O (& MeOH) to determine if these heteroatom tuning trends apply to HFO-sCIs too. To see if the effects observed from heteroatom tuning group XVI-centred co-reactants also apply to group XVII-centred co-reactants, analysis of HFO-sCI + HF & HCl reactions is also included in this section.

3.5.1 HFO-sCI reactions with hydrogen sulphide (H_2S).

The HFO-sCI + H_2S reactions proceed through two hydrogen abstraction transition states to produce hydrosulphide alkyl hydroperoxide, following a reaction process similar to that observed for most sCI + H_2S reactions studied in the computational and experimental literature.[87,136,185] The rate constant for **sCI 1** + H_2S determined here ($k_{THEO} \sim 7.06 \times 10^{-15}$ cm^3 s^{-1}) is larger than that for **sCI 1** + H_2O in this study ($k_{THEO} \sim 1.18 \times 10^{-16}$ cm^3 s^{-1}). This difference in reactivity is substantiated by the fact that a literature k_{EXP} value for **sCI 1** + H_2S observed by Smith *et al.* (1.7×10^{-13} cm^3 s^{-1}) is much larger than the k_{EXP} range observed in the literature for **sCI 1** + H_2O ($0.25–13 \times 10^{-16}$ cm^3 s^{-1}).[64,78,131,136,182,183] When analysing **sCIs 2 & 3** reactions with H_2S each also show much larger k_{THEO} values than their reactions with H_2O, as observed in Fig. 15. Therefore, the theoretical results of H_2S reactions with **sCIs 1–3** help to substantiate the general trend observed by Kumar *et al.* and the experimental literature that, if the central X atomic element of H_2X is substituted with an element further down group XVI on the periodic table, then the k_{THEO} value for the sCI + H_2X reaction increases.[87]

One other point that may be noteworthy is that **sCI 3** & **sCI 1** exhibit similar rate constants throughout all three reactions featured in Fig. 15, as well as throughout much of this study. In much of the literature the non-fluorinated equivalent to **sCI 3**, *anti*-CH_3CHOO, exhibits a higher bimolecular rate constant to **sCI 1** in reactions with H_2O, MeOH & SO_2.[61,74,79,148,151] This may well be due to the presence of hyperconjugative α-H atoms in the *anti*-CH_3 substituent and that α-F atoms on the *anti*-CF_3 group rather than hyperconjugative α-H atoms reduces the inductive impact the substituent has on **sCI 3** reactivity.[56]

In contrast to the patterns seen for the **sCIs 1–3** + H_2S reactions, the rate constants observed for the H_2S reactions with **sCIs 4 & 5** are both smaller than those of the equivalent H_2O reactions (Fig. 15). To determine whether this stagnation of the sCI + H_2S rate constant was due to increased overall steric bulk,

Open Access Article. Published on 17 srpna 2023. Downloaded on 07.01.2026 15:12:46.
This article is licensed under a Creative Commons Attribution 3.0 Unported Licence.

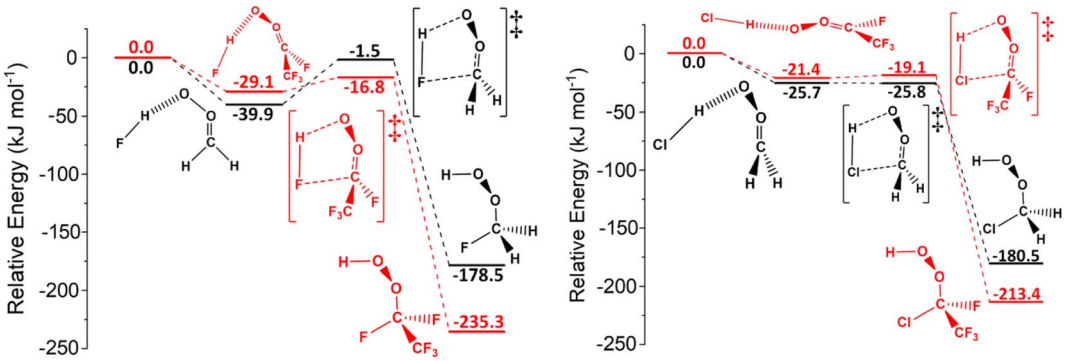

Fig. 16 The potential energy surfaces for selected sCI reactions with HF and HCl. On the potential energy surfaces on the left, feature **sCI 1** + HF, in black, and **sCI 4** + HF, in red. On the potential energy surfaces on the right, feature **sCI 1** + HCl, in black, and **sCI 4** + HCl, in red. Energies are relative to raw reactants.

the k_{THEO} values were for the HFO-sCI reactions with the bulkier MeOH (which also proceeds *via* a hydrogen abstraction mechanism) were determined. However, no such stagnation in the rate constants of **sCI 4** & **5** + MeOH reactions emerges (Fig. 15).

3.5.2 HFO-sCIs reactions with HF & HCl. The Gr17-centred HX compounds, HF & HCl, react with sCIs *via* similar hydrogen abstraction mechanisms as the sCI + H_2X reactions, which means the heteroatom tuning trends seen for the HFO-sCI + H_2X reactions may be replicated.[59,186] For instance, **sCI 1** + HCl has a considerably lower barrier (Fig. 16) to reaction than **sCI 1** + HF, following the trend that the co-reactant with larger heteroatoms (HCl) will have greater reactivity in reactions with **sCIs 1–3**. The resulting k_{THEO} value for **sCI 1** + HF (3.32×10^{-13} cm^3 s^{-1}) is smaller than both the k_{THEO} value (4.70×10^{-10} cm^3 s^{-1}) and its literature k_{EXP} rate constant (1.7×10^{-13} cm^3 s^{-1}) for **sCI 1** + HCl.[59] All **sCIs 1–3** reactions with HCl yield a rate constant that is $\sim 10^3$–10^4 cm^3 s^{-1} larger than the equivalent HFO-sCI + HF reaction, much larger than the equivalent reactivity difference of **sCIs 1–3** + H_2S over that of H_2O ($\sim 10^1$–10^2 cm^3 s^{-1}).

Fig. 16 displays that the fluorinated **sCI 4** has much lower reaction barrier with HF than the unsubstituted **sCI 1** has, demonstrating the continued activating effect that the –F substituent has on the sCI reactivity. The inductive impact of the –F substituent results in **sCI 4** and **sCI 5** having substantially larger rate constants (1.19×10^{-11} & 3.66×10^{-13} cm^3 s^{-1}) compared to the **sCI 1** + HF reaction. In contrast, the energy barrier of the **sCI 4** + HCl reaction does not decrease compared to that of **sCI 1** + HCl (Fig. 16), replicating the observation that heteroatom tuning does not have an inductive effect on reactions involving **sCIs 4** & **5**. In fact, –F substituents in **sCIs 4** & **5** in combination with the heteroatom tuning of the co-reactant leads not just to the same stagnation effect seen for **sCIs 4** & **5** + H_2S reactions, but instead to a reductive effect on reactivity for the **sCIs 4** & **5** + HCl reactions, compared to **sCIs 4** & **5** + HF. This reductive effect is so clear that the rate constants for HCl reactions with **sCI 4** (1.64×10^{-10} cm^3 s^{-1}) and **sCI 5** (1.13×10^{-10} cm^3 s^{-1}) are both smaller than that of the equivalent **sCI 1** reaction for the only time in this study. The cause of these stagnation/reductive effects can potentially be explained in terms of the repulsion between the sCI substituent groups and increased steric interactions, although a deeper exploration into such factors would probably require experimental analysis and verification.[56]

4. Atmospheric implications of HFO-sCIs bimolecular sinks

HFO emissions, and subsequently HFO-sCIs, are projected to become much more abundant as the use of HFO become increasingly widespread in refrigerators, insulation and vehicle cooling units, as is being seen in China, the USA and the EU.[1,27,28] The chemistry of sCIs and other atmospheric species are typically included in atmospheric models in sets of like chemistries or taxonomic groups, where their reactivity can be estimated on the basis of their structure, and this work suggest **sCIs 2–5** can be grouped into any such wider sCI classification system.[40,70,187,188] Similar taxonomic groupings are already used in atmospheric models to estimate the chemistry of large groups of molecules and therefore reduce the computational processing power required to run simulations.[189] However, integrating HFO-sCIs into a wider taxonomic sCI framework faces particular difficulties, principally because of the differing effects non-halogenated groups (–CH_3 and –H) and halogenated groups (–CF_3 and –F) have on the conjugation, hyperconjugation and steric interactions the sCI.[56,72–75] One example of this is the difficulty of including the stagnation/reduction in reactivity of **sCIs 4** & **5** seen during reactions with H_2S & HCl, a phenomenon not exhibited by other sCIs studied here or in the prior literature.[59,64,78,87,131,136,182,183] This shows that system-by-system computational analysis, or indeed ultimately experimental analysis is still vital for understanding the chemistry of many bimolecular sCI reactions.

The effective rate constants, k_{EFF}, a product of the rate constant and the atmospheric abundance of the co-reactant, is used here as a primitive system of measuring the potential tropospheric impact of each bimolecular HFO-sCI reaction studied (Table 1).

The sCI reactions with water are the dominant bimolecular sink for the HFO-sCIs due to the abundance water

© 2023 The Author(s). Published by the Royal Society of Chemistry

Open Access Article. Published on 17 srpna 2023. Downloaded on 07.01.2026 15:12:46.
This article is licensed under a Creative Commons Attribution 3.0 Unported Licence.

vapour.[42,67,68,70,150,179] However, whether the sCI reaction with H_2O or $(H_2O)_2$ is more prevalent depends not only on the relative abundance of the H_2O or $(H_2O)_2$, but also on the identity of the sCI. For instance, the k_{EFF} ($(H_2O)_2$) for **sCI 2** is around 10^3 s^{-1} larger than the equivalent k_{EFF} (H_2O), because the natural abundance of H_2O (6.2×10^{17} molec. per cm^3) over that of $(H_2O)_2$ (8.7×10^{14} molec. per cm^3) is overcome by the fact that the **sCI 2** has a 10^6 cm^3 s^{-1} larger k_{THEO} ($(H_2O)_2$) than k_{THEO} (H_2O). **sCIs 1** & **3** also exhibit larger k_{EFF} ($(H_2O)_2$) than k_{EFF} (H_2O) by between 10^1–10^3 s^{-1}, meaning that tropospheric removal of the sCI occurs more readily *via* reaction with the water dimer than the monomer. But, whereas the rate constants for **sCIs 4** & **5** + H_2O reactions are much enhanced, the **sCIs 4** & **5** + $(H_2O)_2$ systems are so reactive that the k_{d-d} capture limits are used as the rate constants, and the gap between these k_{d-d} ($(H_2O)_2$) and k_{THEO} (H_2O) values is much reduced. Consequently, the k_{EFF} (H_2O) for **sCI 5** is similar to the equivalent k_{EFF} ($(H_2O)_2$) value and the k_{EFF} (H_2O) for **sCI 4** is larger than k_{EFF} ($(H_2O)_2$), as seen in Table 6.

This great preference for HFO-sCI + H_2O & $(H_2O)_2$ reactions leads to the significant production of fluorinated α-hydroxyhydroperoxides, which have been implicated in forest damage and associated with generating important secondary products like H_2O_2, organic acids and aldehydes, albeit that the primary emission locations for HFO are likely to be in urban environments.[86,170–176] HFO-sCI + MeOH reactions are not as competitive as the equivalent H_2O & $(H_2O)_2$ reactions, but because, MeOH is emitted from vehicles that run off biofuel and HFOs are used in vehicle coolant units, the HFO-sCI & MeOH species have greater concentration overlap in many urban environments.[135,190,191] Under such circumstances, emissions of α-alkyoxyalkyl hydroperoxides (AAAHs), a significant functionalised peroxide, are increased and these AAAHs have also been implicated in forest damage and SOA formation.[67,68,78–80,83,86,170]

HFO-sCI reactions with aldehydes are quite uncompetitive compared to the reactions with H_2O & $(H_2O)_2$ but the products of their reactions include organofluoride aldehydes and TFA, both known to contribute to respiratory problems.[192] Furthermore the **sCIs 2–5** reactions with HCHO lead to high yields of **sCI 1** sometimes with a large excess of energy, that easily leads to CI fragmentation and therefore contributes to the tropospheric population of the 'atmospheric detergent' OH radical.[70,82]

The sCI + SO_2 reaction is known to act as a sink for ~20% of some sCIs in boreal forest, however the high uptake of the reactions with H_2O & $(H_2O)_2$ means that they do not contribute hugely to the overall depletion of **sCIs 2–5**.[159] However the SO_2 reactions with **sCIs 2–5** also seem to produce SO_3 at a higher efficiency than reactions with **sCI 1** and $(CH_3)_2COO$, and this tropospheric SO_3 will then contribute to atmospheric H_2SO_4 and aerosol formation.[84,193–196]

TFA may have a disproportionate impact on HFO-sCI bimolecular chemistry because both HFO-sCIs and TFA emerge from the breakdown of HFOs and so they may see a large population overlap with HFO-sCIs. The large rate constants from sCI reactions with TFA, HNO_3 and HCl found here indicate a high reactivity between sCIs and other organic and inorganic acids. However, even in seaside areas, where HCl concentrations are elevated, the contribution that **sCI 1** could make the minor and the role of **sCIs 4** & **5** would be even more reduced, due to the high k_{EFF} values of the sCI + H_2O & $(H_2O)_2$ reactions. The non-water reactions (*e.g.* sCI reactions with HF, SO_2 & H_2S) would contribute more to the depletion of HFO-sCI population in dry environments, such as near active volcanoes.[82,139,197–199]

After collisional stabilisation, sCIs are less energetic so fewer unimolecular fragmentation mechanisms have energy barriers low enough to compete with bimolecular reactions as sinks for sCIs under tropospheric temperature and pressure conditions.[42] According to Guidry *et al.*, the central mechanism for the fragmentation of both *syn*- & *anti*-CF_3CHOO is *via* a 1,3-ring closure to produce a dioxirane ring, both of which produce energy barriers (~80 kJ mol^{-1}) higher than *anti*-CH_3CHOO (~70 kJ mol^{-1}) and more similar to those of CH_2OO (70–100 kJ mol^{-1}).[200] The unimolecular rate constant (k_{UNI}) of

Table 6 A tabulation of the effective rate constants (k_{EFF}) for the HFO-sCI + co-reactant reactions, determined in this study using the product of the theoretical rate constant and the co-reactant abundance. This table shows a primitive calculation of the atmospheric impact of each reaction. If the k_{EFF} value is written in italics, the dipole–dipole capture limit (k_{d-d}) was used to calculate the k_{EFF} value because the master equation rate constant (k_{THEO}) exceeded the k_{d-d} limit or because the reaction was barrierless

	k_{EFF} (s^{-1})				
	CH_2OO	*Syn*-CF_3CHOO	*Anti*-CF_3CHOO	*Syn*-CF_3CFOO	*Anti*-CF_3CFOO
Co-reactant	**sCI 1**	**sCI 2**	**sCI 3**	**sCI 4**	**sCI 5**
HCHO	5.6	0.54	5.0	1447	33.4
SO_2	300	0.79	169	186	183
HNO_3	94	2.3	9.8	58	8.4
TFA	2.5×10^{-2}	1.7×10^{-2}	1.3×10^{-2}	1.2×10^{-2}	1.2×10^{-2}
H_2O	73	0.83	70	3.2×10^6	1.4×10^5
$(H_2O)_2$	2.9×10^3	2.4×10^3	3.3×10^3	6.2×10^5	6.1×10^5
MeOH	0.010	7.9×10^{-5}	0.028	462	28
H_2S	0.085	1.4×10^{-3}	0.042	4.5	0.091
HCl	58	5.0×10^{-3}	8.96	20	14
HF	0.12	2.5×10^{-6}	1.1×10^{-3}	4.4	0.14

Open Access Article. Published on 17 srpna 2023. Downloaded on 07.01.2026 15:12:46.
This article is licensed under a Creative Commons Attribution 3.0 Unported Licence.

a reaction path and k_{EFF} are both equivalent and effective tools to show the efficiency of the respective reaction path as an sCI sink but, while Wang *et al.* have identified *syn*- & *anti*-CF_3CHOO experimentally, no k_{UNI} values were identified in either the Wang *et al.* or Guidry *et al.* studies.[66,200] Therefore, the k_{UNI} for CH_2OO ($\sim$0.3 s^{-1}) is used here instead as it may be the closest analogue to that of *syn*- & *anti*-CF_3CHOO.[42,70] On the basis of these premises, while the k_{UNI} value used here is greater than many of the k_{EFF} value for *syn*- & *anti*-CF_3CHOO found in Table 6, the k_{EFF} value for other reactions, particularly *syn*- & *anti*-CF_3CHOO + $(H_2O)_2$, are greater still. This indicates that bimolecular reactions can compete with unimolecular decomposition.

No equivalent k_{UNI} analogue could be found for *syn*- & *anti*-CF_3CFOO especially considering the role of the –F substituent in CI fragmentation in isolation is also challenging. One study by Ljubić and Sabljić calculated that the *anti*-F substituent induced a lower *anti*-FCHOO fragmentation barrier (TS_{UNI} $\sim$ 47.3 kJ mol^{-1}), whereas *syn*-FCHOO saw no such effect (TS_{UNI} $\sim$ 83.5 kJ mol^{-1}).[201] It is quite possible that the *anti*-F substituent could therefore theoretically induce a higher k_{UNI} for *syn*-CF_3-CFOO, but this might be offset by the lack of any tunnelling effect and the steric hinderance of the *syn*-CF_3 substituent. Nevertheless, no computational or experimental literature exists of the *syn*- & *anti*-CF_3CFOO unimolecular fragmentation reactions, and an assessment of these reactions has been not been deliberated here, due to the need for a more in-depth analysis of these reactions than the kind of provisional evaluation that would be covered in this study.

5. Conclusion

It has been shown that the individual steric and electronic features of HFO-sCIs impact upon their bimolecular chemistry in a way that transcends the choice of tropospheric co-reactant species. The chemistry of **sCI 2** (*syn*-CF_3CHOO) & **sCI 3** (*anti*-CF_3CHOO) have consistency with existing reactivity trends in the literature, particularly that sCIs with a *syn*-orientated sterically bulky group are significantly less reactive than *anti*-orientated sCIs. However, **sCI 3** is distinctive because it exhibits similar rate constants to the unsubstituted **sCI 1** (CH_2OO), whereas sCIs with similar orientations like *anti*-CH_3CHOO yields larger rate constants. The literature indicates that the presence of hyperconjugative α-H atoms in the *anti*-CH_3 group has an inductive impact on the sCI, but here the presence of α-F atoms in the *anti*-CF_3 group appears to reverse this activating effect.

The especially large bimolecular rate constants for **sCI 4** (*syn*-CF_3CFOO) & **sCI 5** (*anti*-CF_3CFOO) emerge from the inductive –F substituents they possess. Moreover, the inductive impact of the –F substituent is greater in the case of **sCI 4** because of the *anti*-position of the –F substituent, and so the k_{THEO} (**sCI 4**) exceeds the k_{THEO} (**sCI 5**). However, with some notable exceptions, the HFO-sCIs studied here follow the reactivity series: k_{THEO} (**sCI 2**) < k_{THEO} (**sCI 3**) $\sim$ k_{THEO} (**sCI 1**) < k_{THEO} (**sCI 5**) < k_{THEO} (**sCI 4**).

One exceptionally distinct observation in this study is that the overall sCI reactivity series is influenced by the choice of co-reactant, as shown when contrasting the reactivity of **sCIs 1–5** reactions with different group-XVI and group-XVII centred co-reactants. When sCI + H_2O & HF are compared with sCI + H_2S & HCl respectively, **sCIs 1–3** reactions with H_2S & HCl produced comparatively larger rate constants, in line with previous literature observations.[87] However, this does not always apply as the –F substituent appear to obstruct the large S and Cl atoms from reaching the reaction site during **sCIs 4** & **5** reactions with H_2S and HCl and this leads to a smaller rate constant.

This work demonstrates that for all sCIs considered, reaction with H_2O or $(H_2O)_2$ is the biggest tropospheric sink of HFO-sCIs, due primarily to the natural abundance of water vapour. Furthermore, these sCI reactions with water produced functionalised hydroxide products called α-hydroxy-hydroperoxide (HHP) that have been implicated with biogenic damage.[42,67,68,78–80,83,86,134,170] While bimolecular reaction with other trace pollutants are less likely to be sinks for HFO-sCIs, **sCIs 2–5** all have a significant capacity to react with tropospheric species such as MeOH, TFA & HNO_3 and yield other functionalised hydroperoxides.

The uncommon nature of these HFO-sCIs is also demonstrated in the multi-step reactions with HCHO, where **sCIs 2–5** react (*via* a short-lived HOZ) to produce another sCI, a highly energised **sCI 1**, a product not commonly found in other studies of sCI + aldehyde reactions.[65,71,147] A similar full mechanistic analysis of the reactions using a two-step HFO-sCI + SO_2 systems show that these reactions have very high rate constants and all produce high yields of SO_3 + R_1R_2CO (0.90–0.99). This production of SO_3 would also lead to H_2SO_4 formation and aerosol nucleation. Furthermore, HFO-sCI reactions with both HCHO & SO_2 systems are found to produce CF_3CHO or CF_3CFO, which are known to contribute to respiratory problems.

In summary, HFO-sCIs are shown to have very unique chemistry, because the –F substituent has a large activation affect on the COO group, whereas the α-F atoms in the CF_3 group are mildly deactivating. If any sCI taxonomic classification is established, **sCIs 2** & **3** could be categorised as part of *syn*-sCI and *anti*-sCI groups respectively, whereas **sCIs 4** & **5** could be categorised in a separate "electronegative substituent" taxonomic group.

Author contributions

The manuscript was written through contributions of all authors. All authors have given approval to the final version of the manuscript.

Conflicts of interest

The authors declare no competing financial interest.

Abbreviations

sCI	Stabilized Criegee intermediate
AAAHs	Alkoxyalkyl hydroperoxides
HHP	Hydroxy-hydroperoxides
HFO-sCIs	Hydrofluoroolefin-derived stabilized Criegee intermediate

© 2023 The Author(s). Published by the Royal Society of Chemistry

Open Access Article. Published on 17 srpna 2023. Downloaded on 07.01.2026 15:12:46.
This article is licensed under a Creative Commons Attribution 3.0 Unported Licence.

TFA	Trifluoracetic acid
HOZ	Heteroozonide
SOZ	Secondary ozonide
NAHP	Nitrooxyalkyl hydroperoxide
HAE	Hydroxyalkyl formate
CH_2OO	**sCI 1**
syn-CF_3CHOO	**sCI 2**
anti-CF_3CHOO	**sCI 3**
syn-CF_3CFOO	**sCI 4**
anti-CF_3CFOO	**sCI 5**

Acknowledgements

This work was partially supported by Advanced Research Computing at Cardiff and High Performance Computing (HPC) Wales, a company formed between the Universities and the private sector in Wales which provides the UK's largest distributed supercomputing network. Dr J. M. Beames was supported in initiating this research through Marie Skłodowska Curie Individual Fellowship NPTC (701593). This work was partially supported by the Natural Environment Research Council (NERC) through the Integrated Research Observation System for Clean Air (OSCA) grant (NE/T001984/1). Information on the data underpinning the results presented here is shown in the ESI.†

References

1 O. US EPA, Refrigerant Transition & Environmental Impacts, **https://www.epa.gov/mvac/refrigerant-transition-environmental-impacts**, accessed 9 January 2019.
2 Fifth Assessment Report - Climate Change 2013, **http://www.ipcc.ch/report/ar5/wg1/**, accessed 26 August 2018.
3 M. K. Vollmer, S. Reimann, M. Hill and D. Brunner, First Observations of the Fourth Generation Synthetic Halocarbons HFC-1234yf, HFC-1234ze(*E*), and HCFC-1233zd(*E*) in the Atmosphere, *Environ. Sci. Technol.*, 2015, **49**, 2703–2708.
4 S. Paul, R. C. Deka and N. K. Gour, Kinetics, mechanism, and global warming potentials of HFO-1234yf initiated by O_3 molecules and NO_3 radicals: insights from quantum study, *Environ. Sci. Pollut. Res.*, 2018, **25**, 26144–26156.
5 P. K. Rao and S. P. Gejji, Atmospheric degradation of HCFO-1233zd(E) initiated by OH radical, Cl atom and O_3 molecule: Kinetics, reaction mechanisms and implications, *J. Fluorine Chem.*, 2018, **211**, 180–193.
6 P. K. Rao and S. P. Gejji, Molecular insights for the HFO-1345fz +X (X = Cl, O_3 or NO_3) reaction and fate of alkoxy radicals initiated by Cl: DFT investigations, *J. Fluorine Chem.*, 2017, **204**, 65–75.
7 C. Arpagaus, F. Bless, M. Uhlmann, E. Büchel, S. Frei, J. Schiffmann and S. Bertsch, *High Temperature Heat Pump Using HFO and HCFO Refrigerants - System Design, Simulation, and First Experimental Results, International Refrigeration and Air Conditioning Conference*, 2018, p. 1875.
8 J. Navarro-Esbrí, A. Fernández-Moreno and A. Mota-Babiloni, Modelling and evaluation of a high-temperature heat pump two-stage cascade with refrigerant mixtures as a fossil fuel boiler alternative for industry decarbonization, *Energy*, 2022, **254**, 124308.
9 T. J. Wallington, M. P. Sulbaek Andersen and O. J. Nielsen, Atmospheric chemistry of short-chain haloolefins: Photochemical ozone creation potentials (POCPs), global warming potentials (GWPs), and ozone depletion potentials (ODPs), *Chemosphere*, 2015, **129**, 135–141.
10 T. J. Wallington, W. F. Schneider, J. Sehested and O. J. Nielsen, Hydrofluorocarbons and stratospheric ozone, *Faraday Discuss.*, 1995, **100**, 55–64.
11 A. R. Ravishankara, A. A. Turnipseed, N. R. Jensen, S. Barone, M. Mills, C. J. Howard and S. Solomon, Do Hydrofluorocarbons Destroy Stratospheric Ozone?, *Science*, 1994, **263**, 71–75.
12 K. O. Patten and D. J. Wuebbles, Atmospheric lifetimes and Ozone Depletion Potentials of trans-1-chloro-3,3,3-trifluoropropylene and trans-1,2-dichloroethylene in a three-dimensional model, *Atmos. Chem. Phys.*, 2010, **10**, 10867–10874.
13 F. P. E. Carré, Improvement in apparatus for freezing liquids, *US Pat.*, US30201A, 1860.
14 F. P. E. Carré, Improvement in ice-machines, *US Pat.*, USRE5287E, 1873.
15 E. C. Smith, Pioneers of Refrigeration, *Nature*, 1943, **151**, 412–413.
16 J. M. Calm, The next generation of refrigerants – Historical review, considerations, and outlook, *Int. J. Refrig.*, 2008, **31**, 1123–1133.
17 E. Askar, V. Schröder, T. Schmid and M. Schwarze, Explosion characteristics of mildly flammable refrigerants ignited with high-energy ignition sources in closed systems, *Int. J. Refrig.*, 2018, **90**, 249–256.
18 Ø. Hodnebrog, M. Etminan, J. S. Fuglestvedt, G. Marston, G. Myhre, C. J. Nielsen, K. P. Shine and T. J. Wallington, Global warming potentials and radiative efficiencies of halocarbons and related compounds: A comprehensive review, *Rev. Geophys.*, 2013, **51**, 300–378.
19 M. J. Molina and F. S. Rowland, Stratospheric sink for chlorofluoromethanes: chlorine atom-catalysed destruction of ozone, *Nature*, 1974, **249**, 810–812.
20 D. L. Narayanan, R. N. Saladi and J. L. Fox, Ultraviolet radiation and skin cancer, *Int. J. Dermatol.*, 2010, **49**, 978–986.
21 Chlorofluorocarbons and Ozone Depletion, **https://www.acs.org/content/acs/en/education/whatischemistry/landmarks/cfcs-ozone.html**, accessed 9 January 2019.
22 The Montreal Protocol, **https://web.archive.org/web/20130602153542/http://ozone.unep.org/new_site/en/montreal_protocol.php**, accessed 4 May 2020.
23 G. J. M. Velders, S. O. Andersen, J. S. Daniel, D. W. Fahey and M. McFarland, The importance of the Montreal Protocol in protecting climate, *Proc. Natl. Acad. Sci. U.S.A.*, 2007, **104**, 4814–4819.
24 R. McKenzie, G. Bernhard, B. Liley, P. Disterhoft, S. Rhodes, A. Bais, O. Morgenstern, P. Newman, L. Oman, C. Brogniez and S. Simic, Success of Montreal Protocol Demonstrated

Open Access Article. Published on 17 srpna 2023. Downloaded on 07.01.2026 15:12:46.
This article is licensed under a Creative Commons Attribution 3.0 Unported Licence.

by Comparing High-Quality UV Measurements with "World Avoided" Calculations from Two Chemistry-Climate Models, *Sci. Rep.*, 2019, **9**, 1–13.

25 O. US EPA, Updating Ozone Calculations and Emissions Profiles for Use in the Atmospheric and Health Effects Framework Model, **https://www.epa.gov/ozone-layer-protection/updating-ozone-calculations-and-emissions-profiles-use-atmospheric-and-health**, accessed 7 August 2020.

26 M. M. Hurwitz, E. L. Fleming, P. A. Newman, F. Li, E. Mlawer, K. Cady-Pereira and R. Bailey, Ozone depletion by hydrofluorocarbons, *Geophys. Res. Lett.*, 2015, **42**, 8686–8692.

27 European Commission - PRESS RELEASES - Press release - Refrigerants used in mobile air condition systems (MAC) - State of play, **http://europa.eu/rapid/press-release_MEMO-14-50_en.htm**, accessed 9 January 2019.

28 B. Zhang, Z. Zhai and J. Zhang, Distribution of trifluoroacetic acid in gas and particulate phases in Beijing from 2013 to 2016, *Sci. Total Environ.*, 2018, **634**, 471–477.

29 Department for Environment, *Food & Rural Affairs, Assessment of the F Gas Regulation in Great Britain*, 2022.

30 J. Soulet, *F-Gas Regulation Could Have Chilling Effect on EU Businesses and Their Customers*, EURACTIV Media network, 2023.

31 N. Everitt, *Industry Urged to Engage with UK F-Gas Survey', Cooling Post*, 2023.

32 D. Fleet, J. Hanlon, K. Osborne, M. La Vedrine and P. Ashford, *Study on Environmental and Health Effects of HFO Refrigerants*, Norwegian Environment Agency, 2017.

33 V. L. Orkin, L. E. Martynova and M. J. Kurylo, Photochemical Properties of *trans*-1-Chloro-3,3,3-trifluoropropene (*trans*-CHCl=CHCF$_3$): OH Reaction Rate Constant, UV and IR Absorption Spectra, Global Warming Potential, and Ozone Depletion Potential, *J. Phys. Chem. A*, 2014, **118**, 5263–5271.

34 M. Antiñolo, I. Bravo, E. Jiménez, B. Ballesteros and J. Albaladejo, Atmospheric Chemistry of *E*- and *Z*-CF$_3$CH=CHF (HFO-1234ze): OH Reaction Kinetics as a Function of Temperature and UV and IR Absorption Cross Sections, *J. Phys. Chem. A*, 2017, **121**, 8322–8331.

35 J. Navarro-Esbrí, M. Amat-Albuixech, F. Molés, C. Mateu-Royo, A. Mota-Babiloni and R. Collado, HCFO-1224yd(Z) as HFC-245fa drop-in alternative in low temperature ORC systems: Experimental analysis in a waste heat recovery real facility, *Energy*, 2020, **193**, 116701.

36 D. J. Luecken, R. L. Waterland, S. Papasavva, K. N. Taddonio, W. T. Hutzell, J. P. Rugh and S. O. Andersen, Ozone and TFA Impacts in North America from Degradation of 2,3,3,3-Tetrafluoropropene (HFO-1234yf), A Potential Greenhouse Gas Replacement, *Environ. Sci. Technol.*, 2010, **44**, 343–348.

37 Honeywell starts up HFO refrigerants plant in Louisiana - Chemical Engineering, **https://www.chemengonline.com/honeywell-starts-up-hfo-refrigerants-plant-in-louisiana/?printmode=1**, accessed 24 October 2018.

38 R. R. Singh, H. T. Pham, D. P. Wilson and R. H.Thomas, Azeotrope-like compositions of tetrafluoropropene and trifluoroiodomethane, *US Pat.*, US6969701B2, 2005.

39 M. Nayak, *U.S. companies brace for climate-friendly alternatives in cooling systems*, Reuters, 2016.

40 M. R. McGillen, T. J. Carey, A. T. Archibald, J. C. Wenger, D. E. Shallcross and C. J. Percival, Structure–activity relationship (SAR) for the gas-phase ozonolysis of aliphatic alkenes and dialkenes, *Phys. Chem. Chem. Phys.*, 2008, **10**, 1757–1768.

41 T. B. Nguyen, G. S. Tyndall, J. D. Crounse, A. P. Teng, K. H. Bates, R. H. Schwantes, M. M. Coggon, L. Zhang, P. Feiner, D. O. Milller, K. M. Skog, J. C. Rivera-Rios, M. Dorris, K. F. Olson, A. Koss, R. J. Wild, S. S. Brown, A. H. Goldstein, J. A. de Gouw, W. H. Brune, F. N. Keutsch, J. H. Seinfeld and P. O. Wennberg, Atmospheric fates of Criegee intermediates in the ozonolysis of isoprene, *Phys. Chem. Chem. Phys.*, 2016, **18**, 10241–10254.

42 M. A. H. Khan, C. J. Percival, R. L. Caravan, C. A. Taatjes and D. E. Shallcross, Criegee intermediates and their impacts on the troposphere, *Environ. Sci.: Processes Impacts*, 2018, **20**, 437–453.

43 R. Atkinson, D. L. Baulch, R. A. Cox, J. N. Crowley, R. F. Hampson, R. G. Hynes, M. E. Jenkin, M. J. Rossi and J. Troe, Evaluated kinetic and photochemical data for atmospheric chemistry: Volume I - gas phase reactions of O_x, HO_x, NO_x and SO_x species, *Atmos. Chem. Phys.*, 2004, **4**, 1461–1738.

44 R. Atkinson, D. L. Baulch, R. A. Cox, R. F. Hampson, J. A. Kerr, M. J. Rossi and J. Troe, Evaluated Kinetic, Photochemical and Heterogeneous Data for Atmospheric Chemistry: Supplement V. IUPAC Subcommittee on Gas Kinetic Data Evaluation for Atmospheric Chemistry, *J. Phys. Chem. Ref. Data*, 1997, **26**, 521–1011.

45 O. J. Nielsen, M. S. Javadi, M. P. Sulbaek Andersen, M. D. Hurley, T. J. Wallington and R. Singh, Atmospheric chemistry of CF_3CFCH_2: Kinetics and mechanisms of gas-phase reactions with Cl atoms, OH radicals, and O_3, *Chem. Phys. Lett.*, 2007, **439**, 18–22.

46 M. P. S. Andersen, E. J. K. Nilsson, O. J. Nielsen, M. S. Johnson, M. D. Hurley and T. J. Wallington, Atmospheric chemistry of trans-$CF_3CHCHCl$: Kinetics of the gas-phase reactions with Cl atoms, OH radicals, and O_3, *J. Photochem. Photobiol., A*, 2008, **199**, 92–97.

47 M. P. S. Andersen, O. J. Nielsen, A. Toft, T. Nakayama, Y. Matsumi, R. L. Waterland, R. C. Buck, M. D. Hurley and T. J. Wallington, Atmospheric chemistry of $C_xF_{2x+1}CHCH_2$ (x=1, 2, 4, 6, and 8): Kinetics of gas-phase reactions with Cl atoms, OH radicals, and O_3, *J. Photochem. Photobiol., A*, 2005, **176**, 124–128.

48 J. G. Calvert, J. J. Orlando, W. R. Stockwell and T. J. Wallington, *The Mechanisms of Reactions Influencing Atmospheric Ozone*, Oxford University Press, 2015.

49 Z. Wang, Y. Wang, J. Li, S. Henne, B. Zhang, J. Hu and J. Zhang, Impacts of the Degradation of 2,3,3,3-Tetrafluoropropene into Trifluoroacetic Acid from Its

© 2023 The Author(s). Published by the Royal Society of Chemistry

Open Access Article. Published on 17 srpna 2023. Downloaded on 07.01.2026 15:12:46.
This article is licensed under a Creative Commons Attribution 3.0 Unported Licence.

Application in Automobile Air Conditioners in China, the United States, and Europe, *Environ. Sci. Technol.*, 2018, **52**, 2819–2826.

50 S. Henne, D. E. Shallcross, S. Reimann, P. Xiao, D. Brunner, S. O'Doherty and B. Buchmann, Future Emissions and Atmospheric Fate of HFC-1234yf from Mobile Air Conditioners in Europe, *Environ. Sci. Technol.*, 2012, **46**, 1650–1658.

51 M. P. Sulbaek Andersen, J. A. Schmidt, A. Volkova and D. J. Wuebbles, A three-dimensional model of the atmospheric chemistry of *E* and *Z*-$CF_3CH{=}CHCl$ (HCFO-1233(zd) (E/Z)), *Atmos. Environ.*, 2018, **179**, 250–259.

52 A. Soto, B. Ballesteros, E. Jiménez, M. Antiñolo, E. Martínez and J. Albaladejo, Kinetic and mechanistic study of the gas-phase reaction of $C_xF_{2x+1}CH{=}CH2$ (x=1, 2, 3, 4 and 6) with O_3 under atmospheric conditions, *Chemosphere*, 2018, **201**, 318–327.

53 R. Søndergaard, O. J. Nielsen, M. D. Hurley, T. J. Wallington and R. Singh, Atmospheric chemistry of trans-$CF_3CHCHCl$: Kinetics of the gas-phase reactions with Cl atoms, OH radicals, and O_3, *Chem. Phys. Lett.*, 2007, **443**, 199–204.

54 M. P. S. Andersen, T. I. Sølling, L. L. Andersen, A. Volkova, D. Hovanessian, C. Britzman, O. J. Nielsen and T. J. Wallington, Atmospheric chemistry of (Z)-$CF_3CHCHCl$: products and mechanisms of the Cl atom, OH radical and O_3 reactions, and role of (E)–(Z) isomerization, *Phys. Chem. Chem. Phys.*, 2018, **20**, 27949–27958.

55 A. Novelli, K. Hens, C. T. Ernest, M. Martinez, A. Nolscher, V. Sinha, P. Paasonen, T. Petaja, M. Sipila, T. Elste and D. Kubistin, *Estimating the Atmospheric Concentration of Criegee Intermediates and Their Possible Interference in a FAGE-LIF Instrument, Faculty of Science, Medicine and Health - Papers*, 2017, pp. 7807–7826.

56 N. Watson, *An Analysis of the Sources and Sinks for Criegee Intermediates: an Extended Computational Study*, Cardiff University, 2021.

57 C. Cabezas, J.-C. Guillemin and Y. Endo, Fourier-transform microwave spectroscopy of a halogen substituted Criegee intermediate ClCHOO, *J. Chem. Phys.*, 2016, **145**, 184304.

58 K. M. Kapnas, B. W. Toulson, E. S. Foreman, S. A. Block, J. G. Hill and C. Murray, UV photodissociation dynamics of CHI_2Cl and its role as a photolytic precursor for a chlorinated Criegee intermediate, *Phys. Chem. Chem. Phys.*, 2017, **19**, 31039–31053.

59 E. S. Foreman, K. M. Kapnas and C. Murray, Reactions between Criegee Intermediates and the Inorganic Acids HCl and HNO_3: Kinetics and Atmospheric Implications, *Angew. Chem., Int. Ed.*, 2016, **55**, 10419–10422.

60 O. Welz, A. J. Eskola, L. Sheps, B. Rotavera, J. D. Savee, A. M. Scheer, D. L. Osborn, D. Lowe, A. Murray Booth, P. Xiao, M. A. H. Khan, C. J. Percival, D. E. Shallcross and C. A. Taatjes, Rate Coefficients of C1 and C2 Criegee Intermediate Reactions with Formic and Acetic Acid Near the Collision Limit: Direct Kinetics Measurements and Atmospheric Implications, *Angew. Chem., Int. Ed.*, 2014, **53**, 4547–4550.

61 R. Chhantyal-Pun, M. R. McGillen, J. M. Beames, M. A. H. Khan, C. J. Percival, D. E. Shallcross and A. J. Orr-Ewing, Temperature-Dependence of the Rates of Reaction of Trifluoroacetic Acid with Criegee Intermediates, *Angew. Chem., Int. Ed.*, 2017, **56**, 9044–9047.

62 M. R. McGillen, B. F. E. Curchod, R. Chhantyal-Pun, J. M. Beames, N. Watson, M. A. H. Khan, L. McMahon, D. E. Shallcross and A. J. Orr-Ewing, Criegee Intermediate–Alcohol Reactions, A Potential Source of Functionalized Hydroperoxides in the Atmosphere, *ACS Earth Space Chem.*, 2017, **1**, 664–672.

63 O. Welz, J. D. Savee, D. L. Osborn, S. S. Vasu, C. J. Percival, D. E. Shallcross and C. A. Taatjes, Direct Kinetic Measurements of Criegee Intermediate (CH_2OO) Formed by Reaction of CH_2I with O_2, *Science*, 2012, **335**, 204–207.

64 D. Stone, M. Blitz, L. Daubney, N. U. M. Howes and P. Seakins, Kinetics of CH_2OO reactions with SO_2, NO_2, NO, H_2O and CH_3CHO as a function of pressure, *Phys. Chem. Chem. Phys.*, 2014, **16**, 1139–1149.

65 C. A. Taatjes, O. Welz, A. J. Eskola, J. D. Savee, D. L. Osborn, E. P. F. Lee, J. M. Dyke, D. W. K. Mok, D. E. Shallcross and C. J. Percival, Direct measurement of Criegee intermediate (CH_2OO) reactions with acetone, acetaldehyde, and hexafluoroacetone, *Phys. Chem. Chem. Phys.*, 2012, **14**, 10391–10400.

66 L. Wang, Z. Wu, B. Lu and X. Zeng, Spectroscopic characterization and photochemistry of the Criegee intermediate $CF_3C(H)OO$, *J. Environ. Sci.*, 2022, **114**, 160–169.

67 J. M. Anglada and A. Solé, Impact of the water dimer on the atmospheric reactivity of carbonyl oxides, *Phys. Chem. Chem. Phys.*, 2016, **18**, 17698–17712.

68 J. M. Anglada, J. González and M. Torrent-Sucarrat, Effects of the substituents on the reactivity of carbonyl oxides. A theoretical study on the reaction of substituted carbonyl oxides with water, *Phys. Chem. Chem. Phys.*, 2011, **13**, 13034–13045.

69 M. Kumar, D. H. Busch, B. Subramaniam and W. H. Thompson, Criegee Intermediate Reaction with CO: Mechanism, Barriers, Conformer-Dependence, and Implications for Ozonolysis Chemistry, *J. Phys. Chem. A*, 2014, **118**, 1887–1894.

70 L. Vereecken, A. Novelli and D. Taraborrelli, Unimolecular decay strongly limits the atmospheric impact of Criegee intermediates, *Phys. Chem. Chem. Phys.*, 2017, **19**, 31599–31612.

71 A. Jalan, J. W. Allen and W. H. Green, Chemically activated formation of organic acids in reactions of the Criegee intermediate with aldehydes and ketones, *Phys. Chem. Chem. Phys.*, 2013, **15**, 16841–16852.

72 M. Kumar and J. S. Francisco, Reactions of Criegee Intermediates with Non-Water Greenhouse Gases: Implications for Metal Free Chemical Fixation of Carbon Dioxide, *J. Phys. Chem. Lett.*, 2017, **8**, 4206–4213.

73 M. Kumar and J. S. Francisco, H–X. (X = H, CH_3, CH_2F, CHF_2, CF_3, and SiH_3) Bond Activation by Criegee

Open Access Article. Published on 17 srpna 2023. Downloaded on 07.01.2026 15:12:46.
This article is licensed under a Creative Commons Attribution 3.0 Unported Licence.

Intermediates: A Theoretical Perspective, *J. Phys. Chem. A*, 2017, **121**, 9421–9428.

74 N. A. I. Watson, J. A. Black, T. M. Stonelake, P. J. Knowles and J. M. Beames, An Extended Computational Study of Criegee Intermediate–Alcohol Reactions, *J. Phys. Chem. A*, 2019, **123**, 218–229.

75 K. Xu, W. Wang, W. Wei, W. Feng, Q. Sun and P. Li, Insights into the Reaction Mechanism of Criegee Intermediate CH_2OO with Methane and Implications for the Formation of Methanol, *J. Phys. Chem. A*, 2017, **121**, 7236–7245.

76 R. Chhantyal-Pun, R. Shannon, D. P. Tew, R. L. Caravan, M. Duchi, C. Wong, A. Ingham, C. Feldman, M. R. McGillen, M. A. H. H. Khan, I. O. Antonov, B. Rotavera, K. Ramasesha, D. L. Osborn, C. A. Taatjes, C. Percival, D. E. Shallcross and A. Orr-Ewing, Experimental and Computational Studies of Criegee Intermediate Reactions with NH_3 and CH_3NH_2, *Phys. Chem. Chem. Phys.*, 2019, **21**, 14042–14052.

77 L. Vereecken, H. Harder and A. Novelli, The reactions of Criegee intermediates with alkenes, ozone, and carbonyl oxides, *Phys. Chem. Chem. Phys.*, 2014, **16**, 4039.

78 W. Chao, J.-T. Hsieh, C.-H. Chang and J. J.-M. Lin, Direct kinetic measurement of the reaction of the simplest Criegee intermediate with water vapor, *Science*, 2015, **347**, 751–754.

79 C. A. Taatjes, O. Welz, A. J. Eskola, J. D. Savee, A. M. Scheer, D. E. Shallcross, B. Rotavera, E. P. F. Lee, J. M. Dyke, D. K. W. Mok, D. L. Osborn and C. J. Percival, Direct Measurements of Conformer-Dependent Reactivity of the Criegee Intermediate CH_3CHOO, *Science*, 2013, **340**, 177–180.

80 M. J. Newland, A. R. Rickard, L. Vereecken, A. Muñoz, M. Ródenas and W. J. Bloss, Atmospheric isoprene ozonolysis: impacts of stabilised Criegee intermediate reactions with SO_2, H_2O and dimethyl sulfide, *Atmos. Chem. Phys.*, 2015, **15**, 9521–9536.

81 G. Ritchie, *Atmospheric Chemistry: from the Surface to the Stratosphere*, World Scientific Publishing Company, 2017.

82 A. M. Holloway and R. P. Wayne, *Atmospheric Chemistry*, Royal Society of Chemistry, 2010.

83 B. Long, J. L. Bao and D. G. Truhlar, Atmospheric Chemistry of Criegee Intermediates: Unimolecular Reactions and Reactions with Water, *J. Am. Chem. Soc.*, 2016, **138**, 14409–14422.

84 K. T. Kuwata, E. J. Guinn, M. R. Hermes, J. A. Fernandez, J. M. Mathison and K. Huang, A Computational Re-examination of the Criegee Intermediate–Sulfur Dioxide Reaction, *J. Phys. Chem. A*, 2015, **119**, 10316–10335.

85 R. Chhantyal-Pun, A. Davey, D. E. Shallcross, C. J. Percival and A. J. Orr-Ewing, A kinetic study of the CH_2OO Criegee intermediate self-reaction, reaction with SO_2 and unimolecular reaction using cavity ring-down spectroscopy, *Phys. Chem. Chem. Phys.*, 2015, **17**, 3617–3626.

86 S. Gäb, E. Hellpointner, W. V. Turner and F. Korte, Hydroxymethyl hydroperoxide and bis(hydroxymethyl) peroxide from gas-phase ozonolysis of naturally occurring alkenes, *Nature*, 1985, **316**, 535–536.

87 M. Kumar and J. S. Francisco, Heteroatom Tuning of Bimolecular Criegee Reactions and Its Implications, *Angew. Chem., Int. Ed.*, 2016, **55**, 13432–13435.

88 A. D. Becke, Density-functional thermochemistry. III. The role of exact exchange, *J. Chem. Phys.*, 1993, **98**, 5648–5652.

89 S. F. Sousa, P. A. Fernandes and M. J. Ramos, General Performance of Density Functionals, *J. Phys. Chem. A*, 2007, **111**, 10439–10452.

90 null Car and null Parrinello, Unified approach for molecular dynamics and density-functional theory, *Phys. Rev. Lett.*, 1985, **55**, 2471–2474.

91 J. Harris and R. O. Jones, The surface energy of a bounded electron gas, *J. Phys. F: Met. Phys.*, 1974, **4**, 1170–1186.

92 J. Poater, M. Duran and M. Solà, Parametrization of the Becke3-LYP hybrid functional for a series of small molecules using quantum molecular similarity techniques, *J. Comput. Chem.*, 2001, **22**, 1666–1678.

93 A. D. Becke, Density-functional exchange-energy approximation with correct asymptotic behavior, *Phys. Rev. A*, 1988, **38**, 3098–3100.

94 C. Lee, W. Yang and R. G. Parr, Development of the Colle-Salvetti correlation-energy formula into a functional of the electron density, *Phys. Rev. B: Condens. Matter Mater. Phys.*, 1988, **37**, 785–789.

95 B. J. Lynch, P. L. Fast, M. Harris and D. G. Truhlar, Adiabatic Connection for Kinetics, *J. Phys. Chem. A*, 2000, **104**, 4811–4815.

96 E. G. Lewars, *Computational Chemistry: Introduction to the Theory and Applications of Molecular and Quantum Mechanics*, Springer Science & Business Media, 2010.

97 T. Kupka and C. Lim, Polarization-Consistent versus Correlation-Consistent Basis Sets in Predicting Molecular and Spectroscopic Properties, *J. Phys. Chem. A*, 2007, **111**, 1927–1932.

98 K. A. Peterson and T. H. Dunning, Accurate correlation consistent basis sets for molecular core–valence correlation effects: The second row atoms Al–Ar, and the first row atoms B–Ne revisited, *J. Chem. Phys.*, 2002, **117**, 10548–10560.

99 D. Feller, K. A. Peterson and T. D. Crawford, Sources of error in electronic structure calculations on small chemical systems, *J. Chem. Phys.*, 2006, **124**, 054107.

100 M. J. Frisch, G. W. Trucks, H. B. Schlegel, G. E. Scuseria, M. A. Robb, J. R. Cheeseman, G. Scalmani, V. Barone, G. A. Petersson, H. Nakatsuji, X. Li, M. Caricato, A. Marenich, J. Bloino, B. G. Janesko, R. Gomperts, B. Mennucci, H. P. Hratchian, J. V. Ortiz, A. F. Izmaylov, J. L. Sonnenberg, D. Williams-Young, F. Ding, F. Lipparini, F. Egidi, J. Goings, B. Peng, A. Petrone, T. Henderson, D. Ranasinghe, V. G. Zakrzewski, J. Gao, N. Rega, G. Zheng, W. Liang, M. Hada, M. Ehara, K. Toyota, R. Fukuda, J. Hasegawa, M. Ishida, T. Nakajima, Y. Honda, O. Kitao, H. Nakai, T. Vreven, K. Throssell, J. A. Montgomery Jr, J. E. Peralta, F. Ogliaro, M. Bearpark, J. J. Heyd, E. Brothers, K. N. Kudin, V. N. Staroverov, T. Keith, R. Kobayashi, J. Normand, K. Raghavachari, A. Rendell, J. C. Burant, S. S. Iyengar,

© 2023 The Author(s). Published by the Royal Society of Chemistry

Open Access Article. Published on 17 srpna 2023. Downloaded on 07.01.2026 15:12:46.
This article is licensed under a Creative Commons Attribution 3.0 Unported Licence.

J. Tomasi, M. Cossi, J. M. Millam, M. Klene, C. Adamo, R. Cammi, J. W. Ochterski, R. L. Martin, K. Morokuma, O. Farkas, J. B. Foresman and D. J. Fox, *Gaussian 09, Revision A.02*, Gaussian, Inc, Wallingford CT, 2016.

101 P. Atkins, J. de Paula and R. Friedman, *Physical Chemistry: Quanta, Matter, and Change*, OUP, Oxford, 2013.

102 D. Spellmeyer, *Annual Reports in Computational Chemistry*, Elsevier, 2006.

103 P. Pulay, Localizability of dynamic electron correlation, *Chem. Phys. Lett.*, 1983, **100**, 151–154.

104 P. Pulay and S. Saebø, Orbital-invariant formulation and second-order gradient evaluation in Møller-Plesset perturbation theory, *Theor. Chim. Acta*, 1986, **69**, 357–368.

105 R. Polly, H.-J. Werner, F. R. Manby and P. J. Knowles, Fast Hartree–Fock theory using local density fitting approximations, *Mol. Phys.*, 2004, **102**, 2311–2321.

106 H.-J. Werner and K. Pflüger, in *Annual Reports in Computational Chemistry*, ed. D. C. Spellmeyer, Elsevier, 2006, vol. 2, pp. 53–80.

107 S. Loibl, F. R. Manby and M. Schütz, Density fitted, local Hartree–Fock treatment of NMR chemical shifts using London atomic orbitals, *Mol. Phys.*, 2010, **108**, 477–485.

108 T. B. Adler and H.-J. Werner, An explicitly correlated local coupled cluster method for calculations of large molecules close to the basis set limit, *J. Chem. Phys.*, 2011, **135**, 144117.

109 T. B. Adler, G. Knizia and H.-J. Werner, A simple and efficient CCSD(T)-F12 approximation, *J. Chem. Phys.*, 2007, **127**, 221106.

110 G. Knizia, T. B. Adler and H.-J. Werner, Simplified CCSD(T)-F12 methods: Theory and benchmarks, *J. Chem. Phys.*, 2009, **130**, 054104.

111 K. Wang, W. Li and S. Li, Generalized Energy-Based Fragmentation CCSD(T)-F12a Method and Application to the Relative Energies of Water Clusters $(H_2O)_{20}$, *J. Chem. Theory Comput.*, 2014, **10**, 1546–1553.

112 H.-J. Werner, P. J. Knowles, G. Knizia, F. R. Manby and M. Schütz, Molpro: a general-purpose quantum chemistry program package: Molpro, *Wiley Interdiscip. Rev.: Comput. Mol. Sci.*, 2012, **2**, 242–253.

113 D. R. Glowacki, C.-H. Liang, C. Morley, M. J. Pilling and S. H. Robertson, MESMER: An Open-Source Master Equation Solver for Multi-Energy Well Reactions, *J. Phys. Chem. A*, 2012, **116**, 9545–9560.

114 S. J. Klippenstein and J. A. Miller, From the Time-Dependent, Multiple-Well Master Equation to Phenomenological Rate Coefficients, *J. Phys. Chem. A*, 2002, **106**, 9267–9277.

115 M. F. Vansco, R. L. Caravan, K. Zuraski, F. A. F. Winiberg, K. Au, N. Trongsiriwat, P. J. Walsh, D. L. Osborn, C. J. Percival, M. A. H. Khan, D. E. Shallcross, C. A. Taatjes and M. I. Lester, Experimental Evidence of Dioxole Unimolecular Decay Pathway for Isoprene-Derived Criegee Intermediates, *J. Phys. Chem. A*, 2020, **124**, 3542–3554.

116 S. Sarkar and B. Bandyopadhyay, Singlet (1Δg) O2 as an Efficient Tropospheric Oxidizing Agent: Gas Phase Reaction with Simplest Criegee Intermediate, *Phys. Chem. Chem. Phys.*, 2020, **22**, 19870–19876.

117 J. Peltola, P. Seal, A. Inkilä and A. Eskola, Time-resolved, broadband UV-absorption spectrometry measurements of Criegee intermediate kinetics using a new photolytic precursor: unimolecular decomposition of CH_2OO and its reaction with formic acid, *Phys. Chem. Chem. Phys.*, 2020, **22**, 11797–11808.

118 B. Long, J. L. Bao and D. G. Truhlar, Rapid unimolecular reaction of stabilized Criegee intermediates and implications for atmospheric chemistry, *Nat. Commun.*, 2019, **10**, 2003.

119 D. Stone, K. Au, S. Sime, D. J. Medeiros, M. Blitz, P. W. Seakins, Z. Decker and L. Sheps, Unimolecular decomposition kinetics of the stabilised Criegee intermediates CH_2OO and CD_2OO, *Phys. Chem. Chem. Phys.*, 2018, **20**, 24940–24954.

120 J. M. Gomez and J. M. C. Plane, Reaction Kinetics of CaOH with H and O_2 and O_2CaOH with O: Implications for the Atmospheric Chemistry of Meteoric Calcium, *ACS Earth Space Chem.*, 2017, **1**, 431–441.

121 S. Canneaux, F. Bohr and E. Henon, KiSThelP: a program to predict thermodynamic properties and rate constants from quantum chemistry results, *J. Comput. Chem.*, 2014, **35**, 82–93.

122 S. A. Carr, T. J. Still, M. A. Blitz, A. J. Eskola, M. J. Pilling, P. W. Seakins, R. J. Shannon, B. Wang and S. H. Robertson, Experimental and Theoretical Study of the Kinetics and Mechanism of the Reaction of OH Radicals with Dimethyl Ether, *J. Phys. Chem. A*, 2013, **117**, 11142–11154.

123 R. J. Shannon, R. L. Caravan, M. A. Blitz and D. E. Heard, A combined experimental and theoretical study of reactions between the hydroxyl radical and oxygenated hydrocarbons relevant to astrochemical environments, *Phys. Chem. Chem. Phys.*, 2014, **16**, 3466–3478.

124 M. A. Blitz, D. Talbi, P. W. Seakins and I. W. M. Smith, Rate Constants and Branching Ratios for the Reaction of CH Radicals with NH_3: A Combined Experimental and Theoretical Study, *J. Phys. Chem. A*, 2012, **116**, 5877–5885.

125 R. Chhantyal-Pun, B. Rotavera, M. R. McGillen, M. A. H. Khan, A. J. Eskola, R. L. Caravan, L. Blacker, D. P. Tew, D. L. Osborn, C. J. Percival, C. A. Taatjes, D. E. Shallcross and A. J. Orr-Ewing, Criegee Intermediate Reactions with Carboxylic Acids: A Potential Source of Secondary Organic Aerosol in the Atmosphere, *ACS Earth Space Chem.*, 2018, **2**, 833–842.

126 A. I. Maergoiz, E. E. Nikitin, J. Troe and V. G. Ushakov, Classical trajectory and adiabatic channel study of the transition from adiabatic to sudden capture dynamics. III. Dipole–dipole capture, *J. Chem. Phys.*, 1996, **105**, 6277–6284.

127 P.-L. Luo, I.-Y. Chen, M. A. H. Khan and D. E. Shallcross, Direct gas-phase formation of formic acid through reaction of Criegee intermediates with formaldehyde, *Commun. Chem.*, 2023, **6**, 1–10.

Open Access Article. Published on 17 srpna 2023. Downloaded on 07.01.2026 15:12:46.
This article is licensed under a Creative Commons Attribution 3.0 Unported Licence.

128 Air quality guidelines for Europe, https://www.euro.who.int/en/publications/abstracts/air-quality-guidelines-for-europe, accessed 22 January 2021.
129 W. Lin, X. Xu, Z. Ma, H. Zhao, X. Liu and Y. Wang, Characteristics and recent trends of sulfur dioxide at urban, rural, and background sites in North China: Effectiveness of control measures, *J. Environ. Sci.*, 2012, **24**, 34–49.
130 Y. J. Leong, A. P. Rutter, H. Y. Wong, C. V. Gutierrez, M. Junaid, E. Scheuer, L. Gong, R. Lewicki, J. E. Dibb, F. K. Tittel and R. J. Griffin, Impact of environmental variables on the reduction of nitric acid by proxies for volatile organic compounds emitted by motor vehicles, *Atmos. Pollut. Res.*, 2016, **7**, 221–227.
131 L. Sheps, B. Rotavera, A. J. Eskola, D. L. Osborn, C. A. Taatjes, K. Au, D. E. Shallcross, M. A. H. Khan and C. J. Percival, The reaction of Criegee intermediate CH_2OO with water dimer: primary products and atmospheric impact, *Phys. Chem. Chem. Phys.*, 2017, **19**, 21970–21979.
132 J. M. Anglada, G. J. Hoffman, L. V. Slipchenko, M. M. Costa, M. F. Ruiz-López and J. S. Francisco, Atmospheric Significance of Water Clusters and Ozone–Water Complexes, *J. Phys. Chem. A*, 2013, **117**, 10381–10396.
133 M. A. Bravo, J. Son, C. U. de Freitas, N. Gouveia and M. L. Bell, Air pollution and mortality in São Paulo, Brazil: Effects of multiple pollutants and analysis of susceptible populations, *J. Exposure Sci. Environ. Epidemiol.*, 2016, **26**, 150–161.
134 S. V. Tadayon, E. S. Foreman and C. Murray, Kinetics of the Reactions between the Criegee Intermediate CH_2OO and Alcohol, *J. Phys. Chem. A*, 2018, **122**, 258–268.
135 H. T.-H. Nguyen, N. Takenaka, H. Bandow, Y. Maeda, S. T. de Oliva, M. M. f. Botelho and T. M. Tavares, Atmospheric alcohols and aldehydes concentrations measured in Osaka, Japan and in Sao Paulo, Brazil, *Atmos. Environ.*, 2001, **35**, 3075–3083.
136 M. C. Smith, W. Chao, M. Kumar, J. S. Francisco, K. Takahashi and J. J.-M. Lin, Temperature-Dependent Rate Coefficients for the Reaction of CH_2OO with Hydrogen Sulfide, *J. Phys. Chem. A*, 2017, **121**, 938–945.
137 National Research Council (US) Committee, Acute Exposure Guideline Levels, *Hydrogen Sulfide Acute Exposure Guideline Levels*, National Academies Press (US), 2010.
138 T. A. Crisp, B. M. Lerner, E. J. Williams, P. K. Quinn, T. S. Bates and T. H. Bertram, Observations of gas phase hydrochloric acid in the polluted marine boundary layer, *J. Geophys. Res.: Atmos.*, 2014, **119**, 6897–6915.
139 M.-D. Cheng, Atmospheric chemistry of hydrogen fluoride, *J. Atmos. Chem.*, 2018, **75**, 1–16.
140 E. V. Avzianova and P. A. Ariya, Temperature-dependent kinetic study for ozonolysis of selected tropospheric alkenes, *Int. J. Chem. Kinet.*, 2002, **34**, 678–684.
141 G. J. Raw, S. K. D. Coward, V. M. Brown and D. R. Crump, Exposure to air pollutants in English homes, *J. Exposure Sci. Environ. Epidemiol.*, 2004, **14**, S85–S94.
142 J. Kazil, S. McKeen, S.-W. Kim, R. Ahmadov, G. A. Grell, R. K. Talukdar and A. R. Ravishankara, Deposition and rainwater concentrations of trifluoroacetic acid in the United States from the use of HFO-1234yf, *J. Geophys. Res.: Atmos.*, 2014, **119**, 14059–14079.
143 A. Tiwary and I. Williams, *Air Pollution: Measurement, Modelling and Mitigation*, CRC Press, 4h edn, 2018.
144 L. Zhu, D. J. Jacob, F. N. Keutsch, L. J. Mickley, R. Scheffe, M. Strum, G. González Abad, K. Chance, K. Yang, B. Rappenglück, D. B. Millet, M. Baasandorj, L. Jaeglé and V. Shah, Formaldehyde (HCHO) As a Hazardous Air Pollutant: Mapping Surface Air Concentrations from Satellite and Inferring Cancer Risks in the United States, *Environ. Sci. Technol.*, 2017, **51**, 5650–5657.
145 J. C. Salamanca, J. Meehan-Atrash, S. Vreeke, J. O. Escobedo, D. H. Peyton and R. M. Strongin, E-cigarettes can emit formaldehyde at high levels under conditions that have been reported to be non-averse to users, *Sci. Rep.*, 2018, **8**, 7559.
146 Q. Ma, X. Lin, C. Yang, B. Long, Y. Gai and W. Zhang, The influences of ammonia on aerosol formation in the ozonolysis of styrene: roles of Criegee intermediate reactions, *R. Soc. Open Sci.*, 2018, **5**, 172171.
147 R. M. I. Elsamra, A. Jalan, Z. J. Buras, J. E. Middaugh and W. H. Green, Temperature- and Pressure-Dependent Kinetics of CH_2OO + CH_3COCH_3 and CH_2OO + CH_3CHO: Direct Measurements and Theoretical Analysis, *Int. J. Chem. Kinet.*, 2016, **48**, 474–488.
148 Y.-H. Lin, K. Takahashi and J. J.-M. Lin, Reactivity of Criegee Intermediates toward Carbon Dioxide, *J. Phys. Chem. Lett.*, 2018, **9**, 184–188.
149 A. B. Ryzhkov and P. A. Ariya, A theoretical study of the reactions of parent and substituted Criegee intermediates with water and the water dimer, *Phys. Chem. Chem. Phys.*, 2004, **6**, 5042–5050.
150 L.-C. Lin, H.-T. Chang, C.-H. Chang, W. Chao, M. C. Smith, C.-H. Chang, J. J.-M. Lin and K. Takahashi, Competition between H_2O and $(H_2O)_2$ reactions with CH_2OO/CH_3CHOO, *Phys. Chem. Chem. Phys.*, 2016, **18**, 4557–4568.
151 L. Sheps, A. M. Scully and K. Au, UV absorption probing of the conformer-dependent reactivity of a Criegee intermediate CH_3CHOO, *Phys. Chem. Chem. Phys.*, 2014, **16**, 26701–26706.
152 T. Berndt, J. Voigtländer, F. Stratmann, H. Junninen, R. L. M. Iii, M. Sipilä, M. Kulmala and H. Herrmann, Competing atmospheric reactions of CH_2OO with SO_2 and water vapour, *Phys. Chem. Chem. Phys.*, 2014, **16**, 19130–19136.
153 L. Sheps, Absolute Ultraviolet Absorption Spectrum of a Criegee Intermediate CH_2OO, *J. Phys. Chem. Lett.*, 2013, **4**, 4201–4205.
154 Y. Liu, K. D. Bayes and S. P. Sander, Measuring Rate Constants for Reactions of the Simplest Criegee Intermediate (CH_2OO) by Monitoring the OH Radical, *J. Phys. Chem. A*, 2014, **118**, 741–747.
155 T. Kurtén, J. R. Lane, S. Jørgensen and H. G. Kjaergaard, A Computational Study of the Oxidation of SO_2 to SO_3 by Gas-

© 2023 The Author(s). Published by the Royal Society of Chemistry

Open Access Article. Published on 17 srpna 2023. Downloaded on 07.01.2026 15:12:46.
This article is licensed under a Creative Commons Attribution 3.0 Unported Licence.

Phase Organic Oxidants, *J. Phys. Chem. A*, 2011, **115**, 8669–8681.

156 Y. Liu, F. Liu, S. Liu, D. Dai, W. Dong and X. Yang, A kinetic study of the CH_2OO Criegee intermediate reaction with SO_2, $(H_2O)_2$, CH_2I_2 and I atoms using OH laser induced fluorescence, *Phys. Chem. Chem. Phys.*, 2017, **19**, 20786–20794.

157 M. C. Smith, C.-H. Chang, W. Chao, L.-C. Lin, K. Takahashi, K. A. Boering and J. J.-M. Lin, Strong Negative Temperature Dependence of the Simplest Criegee Intermediate CH_2OO Reaction with Water Dimer, *J. Phys. Chem. Lett.*, 2015, **6**, 2708–2713.

158 R. Yajima, Y. Sakamoto, S. Inomata and J. Hirokawa, Relative Reactivity Measurements of Stabilized CH_2OO, Produced by Ethene Ozonolysis, Toward Acetic Acid and Water Vapor Using Chemical Ionization Mass Spectrometry, *J. Phys. Chem. A*, 2017, **121**, 6440–6449.

159 L. Vereecken, H. Harder and A. Novelli, The reaction of Criegee intermediates with NO, RO_2, and SO_2, and their fate in the atmosphere, *Phys. Chem. Chem. Phys.*, 2012, **14**, 14682–14695.

160 M. Hallquist, J. C. Wenger, U. Baltensperger, Y. Rudich, D. Simpson, M. Claeys, J. Dommen, N. M. Donahue, C. George, A. H. Goldstein, J. F. Hamilton, H. Herrmann, T. Hoffmann, Y. Iinuma, M. Jang, M. E. Jenkin, J. L. Jimenez, A. Kiendler-Scharr, W. Maenhaut, G. McFiggans, T. F. Mentel, A. Monod, A. S. H. Prévôt, J. H. Seinfeld, J. D. Surratt, R. Szmigielski and J. Wildt, The formation, properties and impact of secondary organic aerosol: current and emerging issues, *Atmos. Chem. Phys.*, 2009, **9**, 5155–5236.

161 O. US EPA, Benefits and Costs of the Clean Air Act 1990-2020, Report Documents and Graphics, **https://www.epa.gov/clean-air-act-overview/benefits-and-costs-clean-air-act-1990-2020-report-documents-and-graphics**, accessed 20 July 2020.

162 D. Huang, J. Xu and S. Zhang, Valuing the health risks of particulate air pollution in the Pearl River Delta, China, *Environ. Sci. Policy*, 2012, **15**, 38–47.

163 J. Wang, S. Wang, A. S. Voorhees, B. Zhao, C. Jang, J. Jiang, J. S. Fu, D. Ding, Y. Zhu and J. Hao, Assessment of short-term PM2.5-related mortality due to different emission sources in the Yangtze River Delta, China, *Atmos. Environ.*, 2015, **123**, 440–448.

164 J. Baek, Y. Hu, M. T. Odman and A. G. Russell, Modeling secondary organic aerosol in CMAQ using multigenerational oxidation of semi-volatile organic compounds, *J. Geophys. Res.: Atmos.*, 2015, **116**, 22204–22216.

165 Z. Ren-Jian, H. Kin-Fai and S. Zhen-Xing, The Role of Aerosol in Climate Change, the Environment, and Human Health, *Atmos. Ocean. Sci. Lett.*, 2015, **5**(2), 156–161.

166 T. Berndt, H. Herrmann and T. Kurtén, Direct Probing of Criegee Intermediates from Gas-Phase Ozonolysis Using Chemical Ionization Mass Spectrometry, *J. Am. Chem. Soc.*, 2017, **139**, 13387–13392.

167 E. Sanhueza, Hydrochloric acid from chlorocarbons: a significant global source of background rain acidity, *Tellus B*, 2001, **53**, 122–132.

168 P. Raghunath, Y.-P. Lee and M. C. Lin, Computational Chemical Kinetics for the Reaction of Criegee Intermediate CH_2OO with HNO_3 and Its Catalytic Conversion to OH, *J. Phys. Chem. A*, 2017, **121**, 3871–3878.

169 L. Vereecken, The reaction of Criegee intermediates with acids and enols, *Phys. Chem. Chem. Phys.*, 2017, **19**, 28630–28640.

170 K. H. Becker, K. J. Brockmann and J. Bechara, Production of hydrogen peroxide in forest air by reaction of ozone with terpenes, *Nature*, 1990, **346**, 256–258.

171 P. Neeb, F. Sauer, O. Horie and G. K. Moortgat, Formation of hydroxymethyl hydroperoxide and formic acid in alkene ozonolysis in the presence of water vapour, *Atmos. Environ.*, 1997, **31**, 1417–1423.

172 F. Sauer, C. Schäfer, P. Neeb, O. Horie and G. K. Moortgat, Formation of hydrogen peroxide in the ozonolysis of isoprene and simple alkenes under humid conditions, *Atmos. Environ.*, 1999, **33**, 229–241.

173 O. Horie and G. K. Moortgat, Gas-Phase Ozonolysis of Alkenes. Recent Advances in Mechanistic Investigations, *Acc. Chem. Res.*, 1998, **31**, 387–396.

174 R. Crehuet, J. M. Anglada and J. M. Bofill, Tropospheric Formation of Hydroxymethyl Hydroperoxide, Formic Acid, H_2O_2, and OH from Carbonyl Oxide in the Presence of Water Vapor: A Theoretical Study of the Reaction Mechanism, *Chem.–Eur. J.*, 2001, **7**, 2227–2235.

175 E. Jiménez, S. González, M. Cazaunau, H. Chen, B. Ballesteros, V. Daële, J. Albaladejo and A. Mellouki, Atmospheric Degradation Initiated by OH Radicals of the Potential Foam Expansion Agent, $CF_3(CF_2)_2CH{=}CH_2$ (HFC-1447fz): Kinetics and Formation of Gaseous Products and Secondary Organic Aerosols, *Environ. Sci. Technol.*, 2016, **50**, 1234–1242.

176 P. Aplincourt and J. M. Anglada, Theoretical Studies on Isoprene Ozonolysis under Tropospheric Conditions. 1. Reaction of Substituted Carbonyl Oxides with Water, *J. Phys. Chem. A*, 2003, **107**, 5798–5811.

177 L. Chen, Y. Huang, Y. Xue, Z. Shen, J. Cao and W. Wang, Mechanistic and kinetics investigations of oligomer formation from Criegee intermediate reactions with hydroxyalkyl hydroperoxides, *Atmos. Chem. Phys.*, 2019, **19**, 4075–4091.

178 Z. J. Buras, R. M. I. Elsamra, A. Jalan, J. E. Middaugh and W. H. Green, Direct Kinetic Measurements of Reactions between the Simplest Criegee Intermediate CH_2OO and Alkenes, *J. Phys. Chem. A*, 2014, **118**, 1997–2006.

179 L.-C. Lin, W. Chao, C.-H. Chang, K. Takahashi and J. J.-M. Lin, Temperature dependence of the reaction of *anti*-CH_3CHOO with water vapor, *Phys. Chem. Chem. Phys.*, 2016, **18**, 28189–28197.

180 S. Bauerle and G. K. Moortgat, Absorption cross-sections of $HOCH_2OOH$ vapor between 205 and 360 nm at 298 K, *Chem. Phys. Lett.*, 1999, **309**, 43–48.

Open Access Article. Published on 17 srpna 2023. Downloaded on 07.01.2026 15:12:46.
This article is licensed under a Creative Commons Attribution 3.0 Unported Licence.

181 H. M. Allen, J. D. Crounse, K. H. Bates, A. P. Teng, M. P. Krawiec-Thayer, J. C. Rivera-Rios, F. N. Keutsch, J. M. St. Clair, T. F. Hanisco, K. H. Møller, H. G. Kjaergaard and P. O. Wennberg, Kinetics and Product Yields of the OH Initiated Oxidation of Hydroxymethyl Hydroperoxide, *J. Phys. Chem. A*, 2018, **122**, 6292–6302.

182 B. Ouyang, M. W. McLeod, R. L. Jones and W. J. Bloss, NO_3 radical production from the reaction between the Criegee intermediate CH_2OO and NO_2, *Phys. Chem. Chem. Phys.*, 2013, **15**, 17070–17075.

183 T. Berndt, R. Kaethner, J. Voigtländer, F. Stratmann, M. Pfeifle, P. Reichle, M. Sipilä, M. Kulmala and M. Olzmann, Kinetics of the unimolecular reaction of CH_2OO and the bimolecular reactions with the water monomer, acetaldehyde and acetone under atmospheric conditions, *Phys. Chem. Chem. Phys.*, 2015, **17**, 19862–19873.

184 T. R. Lewis, M. A. Blitz, D. E. Heard and P. W. Seakins, Direct evidence for a substantive reaction between the Criegee intermediate, CH_2OO, and the water vapour dimer, *Phys. Chem. Chem. Phys.*, 2015, **17**, 4859–4863.

185 M. Kumar, J. Zhong, J. S. Francisco and X. C. Zeng, Criegee intermediate-hydrogen sulfide chemistry at the air/water interface, *Chem. Sci.*, 2017, **8**, 5385–5391.

186 S. Liu, X. Zhou, Y. Chen, Y. Liu, S. Yu, K. Takahashi, H. Ding, Z. Ding, X. Yang and W. Dong, Experimental and Computational Studies of Criegee Intermediate *syn*-CH_3CHOO Reaction with Hydrogen Chloride, *J. Phys. Chem. A*, 2021, **125**, 8587–8594.

187 M. R. McGillen, A. T. Archibald, T. Carey, K. E. Leather, D. E. Shallcross, J. C. Wenger and C. J. Percival, Structure–activity relationship (SAR) for the prediction of gas-phase ozonolysis rate coefficients: an extension towards heteroatomic unsaturated species, *Phys. Chem. Chem. Phys.*, 2011, **13**, 2842–2849.

188 K. E. Leather, M. R. McGillen and C. J. Percival, Temperature-dependent ozonolysis kinetics of selected alkenes in the gas phase: an experimental and structure–activity relationship (SAR) study, *Phys. Chem. Chem. Phys.*, 2010, **12**, 2935–2943.

189 R. Sommariva, S. Cox, C. Martin, K. Borońska, J. Young, P. Jimack, M. J. Pilling, V. N. Matthaios, M. J. Newland, M. Panagi, W. J. Bloss, P. S. Monks and A. R. Rickard, AtChem, an open source box-model for the Master Chemical Mechanism, *Geosci. Model Dev.*, 2019, 1–27.

190 J. Pu, H. Xu, B. Yao, Y. Yu, Y. Jiang, Q. Ma and L. Chen, Estimate of Hydrofluorocarbon Emissions for 2012–16 in the Yangtze River Delta, China, *Adv. Atmos. Sci.*, 2020, **37**, 576–585.

191 É. C. M. de Lanes, P. M. de A. Costa and S. Y. Motoike, Alternative fuels, **https://www.nature.com/articles/511031a**, accessed 27 March 2018.

192 *Committee on Acute Exposure Guideline Levels, Committee on Toxicology, Board on Environmental Studies and Toxicology; Division on Earth and Life Studies and National Research Council, Acute Exposure Guideline Levels for Selected Airborne Chemicals*, National Academies Press (US), 2012, vol. 13.

193 R. L. Mauldin III, T. Berndt, M. Sipilä, P. Paasonen, T. Petäjä, S. Kim, T. Kurtén, F. Stratmann, V.-M. Kerminen and M. Kulmala, A new atmospherically relevant oxidant of sulphur dioxide, *Nature*, 2012, **488**, 193–196.

194 R. A. Cox and S. A. Penkett, Oxidation of Atmospheric SO_2 by Products of the Ozone–Olefin Reaction, *Nature*, 1971, **230**, 321–322.

195 M. Jang, N. M. Czoschke, S. Lee and R. M. Kamens, Heterogeneous Atmospheric Aerosol Production by Acid-Catalyzed Particle-Phase Reactions, *Science*, 2002, **298**, 814–817.

196 M. Boy, D. Mogensen, S. Smolander, L. Zhou, T. Nieminen, P. Paasonen, C. Plass-Dülmer, M. Sipilä, T. Petäjä, L. Mauldin, H. Berresheim and M. Kulmala, Oxidation of SO_2 by stabilized Criegee intermediate (sCI) radicals as a crucial source for atmospheric sulfuric acid concentrations, *Atmos. Chem. Phys.*, 2013, **13**, 3865–3879.

197 T. A. Mather, Volcanoes and the environment: Lessons for understanding Earth's past and future from studies of present-day volcanic emissions, *J. Volcanol. Geotherm. Res.*, 2015, **304**, 160–179.

198 A. Carfora, C. P. Campobasso, P. Cassandro, F. La Sala, A. Maiellaro, A. Perna, R. Petrella and R. Borriello, Fatal inhalation of volcanic gases in three tourists of a geothermal area, *Forensic Sci. Int.*, 2019, **297**, e1–e7.

199 A. Aiuppa, A. Franco, R. von Glasow, A. G. Allen, W. D'Alessandro, T. A. Mather, D. M. Pyle and M. Valenza, The tropospheric processing of acidic gases and hydrogen sulphide in volcanic gas plumes as inferred from field and model investigations, *Atmos. Chem. Phys.*, 2007, **7**, 1441–1450.

200 L. M. Guidry, C. A. Poirier, J. M. Ratliff, E. Antwi, B. Marchetti and T. N. V. Karsili, Modeling the Unimolecular Decay Dynamics of the Fluorinated Criegee Intermediate, CF3CHOO, *Photochem*, 2023, **3**, 327–335.

201 I. Ljubić and A. Sabljić, Fluorocarbonyl oxide: CASSCF/CASPT2 study of structure, cis effect and unimolecular decomposition paths, *Chem. Phys.*, 2005, **309**, 157–165.

© 2023 The Author(s). Published by the Royal Society of Chemistry